

1  
2  
3  
4  
5  
6  
7  
8  
9  
10  
11  
12

# **Reactive Uptake of Ammonia to Secondary Organic Aerosols: Kinetics of Organonitrogen Formation**

Yongchun Liu<sup>1,2</sup>, John Liggi<sup>1\*</sup> and Ralf Staebler<sup>1</sup>, Shao-Meng Li<sup>1</sup>

1. Atmospheric Science and Technology Directorate, Science and Technology

Branch, Environment Canada, Toronto, M3H 5T4, Canada

2. State Key Joint Laboratory of Environment Simulation and Pollution

Control, Research Center for Eco-Environmental Sciences, Chinese

Academy of Sciences, Beijing, 100085, China

---

\* Corresponding author. Phone: 1-416-739-4840; fax: 1-416-739-4281;  
E-mail: [John.Liggio@ec.gc.ca](mailto:John.Liggio@ec.gc.ca)

13 **Abstract:**

14 As a class of brown carbon, organonitrogen compounds originating from the  
15 heterogeneous uptake of NH<sub>3</sub> by secondary organic aerosol (SOA) have received  
16 significant attention recently. In the current work, particulate organonitrogen formation  
17 during the ozonolysis of  $\alpha$ -pinene and the OH oxidation of m-xylene in the presence of  
18 ammonia (34-125 ppb) was studied in a smog chamber equipped with a High  
19 Resolution Time-of-Flight Aerosol Mass Spectrometer and a Quantum Cascade Laser  
20 instrument. A large diversity of nitrogen containing organic (NOC) fragments was  
21 observed which were consistent with the reactions between ammonia and carbonyl  
22 containing SOA. Ammonia uptake coefficients onto SOA which led to organonitrogen  
23 compounds were reported for the first time, and were in the range of  $\sim 10^{-3}$ - $10^{-2}$ ,  
24 decreasing significantly to  $< 10^{-5}$  after 6 hours of reaction. At the end of experiments  
25 (~6 hr) the NOC mass contributed  $8.9 \pm 1.7$  wt% and  $31.5 \pm 4.4$  wt% to the total  $\alpha$ -pinene  
26 and m-xylene derived SOA, respectively, and 4 – 15 wt% of the total nitrogen in the  
27 system. Uptake coefficients were also found to be positively correlated with particle  
28 acidity and negatively correlated with NH<sub>3</sub> concentration, indicating that heterogeneous  
29 reactions were responsible for the observed NOC mass, possibly limited by liquid phase  
30 diffusion. Under these conditions, the data also indicate that the formation of NOC can  
31 compete kinetically with inorganic acid neutralization. The formation of NOC in this  
32 study suggests that a significant portion of the ambient particle associated N may be  
33 derived from NH<sub>3</sub> heterogeneous reactions with SOA. NOC from such a mechanism  
34 may be an important and unaccounted for source of PM associated nitrogen. This

35 mechanism may also contribute to the medium or long-range transport and wet/dry  
36 deposition of atmospheric nitrogen.

37

## 38 **1.0 Introduction**

39 Black carbon (BC) and brown carbon (BrC) are the most abundant and effective  
40 light absorbing components in atmospheric particles (Stocker et al., 2013;Andreae and  
41 Gelencser, 2006). While BC has been extensively studied (Cappa et al., 2012;Bond et  
42 al., 2013), BrC is currently receiving significant attention from the atmospheric  
43 chemistry community as it is often more abundant than BC in the atmosphere, and has  
44 the potential to be an important climate forcing agent via direct absorption of light  
45 (Laskin et al., 2015). BrC refers to organic matter in atmospheric particles that absorb  
46 light with a strong wavelength dependence (Andreae and Gelencser, 2006;Alexander et  
47 al., 2008;Moise et al., 2015). It exists in various forms, such as soil derived humic  
48 materials, humic-like substances (HULIS), organic materials from combustion  
49 processes, bioaerosols (Andreae and Gelencser, 2006;Salma et al., 2010) and secondary  
50 formation in the atmosphere (Laskin et al., 2015;Zarzana et al., 2012;Nguyen et al.,  
51 2013;Powelson et al., 2014). Although the chemical composition of BrC is highly  
52 complex, light absorption by BrC in the ultraviolet-visible region, quantified by the  
53 mass absorption coefficient (MAC) (typically in the range of 0.001-0.1 m<sup>2</sup> g<sup>-1</sup> at 500  
54 nm of wavelength (Updyke et al., 2012), is ascribed to the  $\pi$ - $\pi^*$  and n- $\pi^*$  bond  
55 transitions of electrons in the chemicals present. The  $\pi$ - $\pi^*$  transition is usually observed  
56 in species with unsaturated bonds, while n- $\pi^*$  transitions are relevant to heteroatoms

57 coupled to unsaturated bonds.

58 Primary emissions of biomass burning particles are regarded as an important source  
59 of BrC (Saleh et al., 2013;Andreae and Gelencser, 2006) since polycyclic aromatic  
60 hydrocarbons (PAHs), nitro-PAHs, oxy-PAHs and other aromatic hydrocarbons, and  
61 therefore unsaturated bonds, are abundant in these combustion particles (Andrade-Eiroa  
62 et al., 2010;Kinsey et al., 2011;Souza et al., 2014). Secondary formation of particulate  
63 organics have also recently been considered another possible source of BrC through  
64 heterogeneous or multiphase chemical reactions (Updyke et al., 2012;Zarzana et al.,  
65 2012;Nguyen et al., 2013;Powelson et al., 2014), in which heteroatoms including O, S,  
66 and N can be introduced into the particulate matter via a variety of precursors. For  
67 example, as characteristic components of HULIS (Nguyen et al., 2014;Nguyen et al.,  
68 2012), organosulfates and organonitrates have been observed in both laboratory  
69 generated (Liggio and Li, 2006b;Iinuma et al., 2009;Russell et al., 2011;Darer et al.,  
70 2011) and ambient organic particles (Hawkins et al., 2010;Surratt et al., 2006;Russell  
71 et al., 2011). Oxygen and nitrogen-containing oligomers of high molecular weight have  
72 also been identified in secondary organic aerosols (SOA) (Kalberer et al., 2004).

73 N-containing organic compounds (NOC) are an important class of heteroatom  
74 containing BrC compounds and can account for an appreciable fraction of organic  
75 aerosol mass (Beddows et al., 2004;Cheng et al., 2006;Kourtchev et al., 2014) which  
76 has been mainly attributed to biomass burning and cooking emissions (Cheng et al.,  
77 2006). As summarized in detail in a recent review paper (Zhang et al., 2015),  
78 heterogeneous reactions, which include acid-base reactions between amines and

79 organic acids as well as acid-catalyzed reactions of carbonyl groups in OA with primary  
80 and secondary amines, are increasingly being considered an important source of particle  
81 bound organonitrogen compounds. For example, acid-base reactions between ammonia  
82 or amines and acid moieties (Liu et al., 2012b;Kuwata and Martin, 2012;Zhang et al.,  
83 2015) or exchange reactions of amines with inorganic ammonium salts (Chan and Chan,  
84 2012;Bzdek et al., 2010;Qiu et al., 2011;Liu et al., 2012a) can lead to the formation of  
85 particle bound ammonium salts. **Reaction to form Schiff base** and/or Mannich reaction  
86 between  $\text{NH}_3$ , ammonium salts or amines with carbonyl functional groups in particles  
87 can also form organonitrogen compounds (Zhang et al., 2015), in which N atoms can  
88 be coupled to double bonds (imines) and act as effective chromophors since both  $\pi$ - $\pi^*$   
89 and  $n$ - $\pi^*$  transitions are possible (Nguyen et al., 2013). It has also been proposed that  
90 Mannich reactions may be a possible formation mechanism for the high-molecular  
91 weight nitrogen-containing organic species observed in ambient particles (Wang et al.,  
92 2010b). Although it has not been confirmed with ambient data, the formation of light  
93 absorbing compounds has been inferred in laboratory studies during reactions between  
94 glyoxal, methylglyoxal and primary amines glycine, methylamine and ammonium  
95 (Zarzana et al., 2012;Yu et al., 2011;Powelson et al., 2014;Lee et al., 2013a;Trainic et  
96 al., 2011). Visible light absorption has also been observed from the reactions between  
97  $\text{O}_3/\text{OH}$  initiated biogenic and anthropogenic SOA and  $\text{NH}_3$  (Updyke et al.,  
98 2012;Nguyen et al., 2013;Lee et al., 2013b;Bones et al., 2010). Using High Resolution  
99 Time-of-Flight Aerosol Mass Spectrometry (HR-ToF-AMS) and Desorption  
100 Electrospray Ionization Mass Spectrometry (DESI-MS), characteristic fragments

101 containing nitrogen ( $C_xH_yN_n$  and  $C_xH_yO_zN_n$ ) from the above reactions have been  
102 identified (Galloway et al., 2009;Laskin et al., 2010;Lee et al., 2013a). Recent studies  
103 have found that BrC produced via such reactions is unstable with respect to degradation  
104 by oxidants (Sareen et al., 2013) and sunlight (Lee et al., 2014;Zhao et al., 2015).  
105 Regardless, NOC are likely to have very interesting chemical properties and  
106 atmospheric implications.

107 In addition to the noted role of organonitrogen in BrC, heterogeneously formed  
108 organonitrogen may be an important nutrient to ecosystems via nitrogen (N) deposition  
109 from the atmosphere (Liu et al., 2013). Heterogeneous reactions leading to NOC can  
110 be considered a process whereby gas-phase nitrogen compounds such as  $NH_3$  or amines  
111 with short lifetimes (via deposition) (Liggio et al., 2011) are transformed to particle-  
112 phase nitrogen compounds with increased atmospheric lifetimes. The subsequent  
113 transport and deposition of particle-phase organonitrogen compounds (rather than gas-  
114 phase N) may have an impact on regional nitrogen cycles by altering N deposition  
115 patterns. However, this process has generally not been considered in current deposition  
116 models (García-Gómez et al., 2014) due to limited knowledge on the formation kinetics  
117 and mechanisms of NOC formation from heterogeneous reactions.

118 While reactions of amines have been implicated as a source of particulate-phase  
119 reduced nitrogen (Zarzana et al., 2012), their ambient gaseous concentrations are  
120 typically low (Cornell et al., 2003).  $NH_3$  is the most abundant form of gas-phase  
121 reduced nitrogen in the atmosphere with global emissions estimated at greater than 33  
122  $Tg(N) yr^{-1}$  (Reis et al., 2009) and typical ambient concentration of several ppbv (Cornell

123 et al., 2003;Heald et al., 2012). As qualitatively confirmed by mass spectrometry in  
124 various experiments (Updyke et al., 2012;Nguyen et al., 2013;Lee et al., 2013b;Bones  
125 et al., 2010), reactions between NH<sub>3</sub> and OA are possible in the atmosphere leading to  
126 particulate reduced nitrogen. In order to assess and model the impacts of **the reaction to**  
127 **form Schiff base**, Mannich or other NOC forming reactions (via NH<sub>3</sub>) on the radiative  
128 forcing potentials of ambient SOA and N-deposition, the kinetics of such reactions are  
129 required, and yet they remain largely unknown. To the best of our knowledge, there is  
130 only one paper which reported the formation rate constant of imidazole-2-  
131 caroxaldehyde (IC) to be  $(2.01\pm 0.40)\times 10^{-12} \text{ M}^{-2} \text{ s}^{-1}$  for the reaction between glyoxal and  
132 aqueous (NH<sub>4</sub>)<sub>2</sub>SO<sub>4</sub> in an effort to simulate cloud processing (Yu et al., 2011).

133 In this study, heterogeneous reactive uptake coefficients ( $\gamma$ ) for NH<sub>3</sub> onto laboratory  
134 SOA, which lead to the formation of particulate NOC, were derived using a smog  
135 chamber coupled to a HR-ToF-AMS. The influence of VOC precursors, seed particle  
136 acidity/composition and gaseous NH<sub>3</sub> concentration on the obtained uptake coefficients  
137 of NH<sub>3</sub> is also investigated. Finally, the implications of the kinetics on atmospheric BrC  
138 and N-deposition are also discussed.

139

## 140 **2.0 EXPERIMENTAL DETAILS**

### 141 **2.1 Chamber experiments.**

142 Experiments were performed in a 9 m<sup>3</sup> cylindrical smog chamber, which has been  
143 described in detail by Bunce et al. (1997). Briefly, this reactor is constructed with 50  
144  $\mu\text{m}$  FEP Teflon film and housed in an air-conditioned room (295 $\pm$ 2 K). The surface-to-

145 volume (S/V) ratio is  $2.7 \text{ m}^{-1}$ . Twenty four black light lamps (Sylvania, F40/350BL)  
146 were installed outside the reactor for photochemical reactions. Before each experiment,  
147 the chamber was cleaned by irradiation (300-400 nm, 350 nm peak wavelength) for 8  
148 hours followed by continuous flushing with zero air for 24 hours, after which the  
149 concentration of particles and ammonia was  $<1 \text{ particle cm}^{-3}$  and  $\sim 5 \text{ ppbv}$ , respectively.

150 A summary of initial experimental conditions is given in Table 1.  $\text{Na}_2\text{SO}_4/\text{H}_2\text{SO}_4$   
151 particles were generated as seeds via atomization (model 3706, TSI), dried through a  
152 diffusion drier, and size-selected with a differential mobility analyzer (DMA) (model,  
153 3081, TSI) to have a mode mobility diameter ( $D_m$ ) of  $\sim 90 \text{ nm}$ . A high concentration of  
154  $\text{Na}_2\text{SO}_4/\text{H}_2\text{SO}_4$  seeds ( $\sim 5000 \text{ particle cm}^{-3}$ ) was added into the chamber to suppress new  
155 particle formation from the added VOC precursor and oxidant. As shown in Figure S2,  
156 new particle formation was suppressed during subsequent SOA formation.  $\alpha$ -pinene or  
157 m-xylene (Sigma Aldrich) were added into the chamber via a syringe which was purged  
158 with zero air prior to use. The VOC concentrations were measured online with a High  
159 Resolution Time-of-Flight Proton Transfer Reaction Mass Spectrometry (HR-ToF-  
160 PTRMS, Ionic Analytic). SOA was formed via the oxidation of the VOCs by  $\text{O}_3$  or OH.  
161 The concentration, size and composition of SOA coated on the seed particles were  
162 measured with a Scanning Mobility Particle Sizer (SPMS, TSI) and a HR-ToF-AMS  
163 (Aerodyne) (DeCarlo et al., 2006) operated alternately in both V- and W-mode. HR-  
164 ToF-AMS data were analyzed with the software PIKA 1.12 (DeCarlo et al., 2006; Aiken  
165 et al., 2007). The concentration of NOC was determined by fitting peaks including those  
166 from the  $\text{NH}_x$ ,  $\text{NO}_x$ ,  $\text{C}_x\text{H}_y\text{N}_n$ ,  $\text{C}_x\text{H}_y\text{ON}_n$  and  $\text{C}_x\text{H}_y\text{O}_2\text{N}_n$  fragment groups. Particle wall



167 loss was accounted for by normalizing SOA and NOC concentrations to the sulfate seed  
168 signal from the HR-ToF-AMS. It should be noted that the NOC concentration may be  
169 underestimated in this study since one cannot resolve all the nitrogen containing  
170 fragments that may exist, and since some of the NOCs may fragment into masses that  
171 do not contain nitrogen and thus are quantified as organic. Furthermore, the relative  
172 ionization efficiency (RIE) for the NOC fragments was assumed to be equivalent to the  
173 remainder of the organics (1.4), since a RIE value for NOC is unknown. This may  
174 introduce an additional uncertainty to the quantitation of NOC. It should also be pointed  
175 out that some NOC species may be formed through the pyrolysis/ionization processes  
176 occurring in the ionization region. This would result in a positive uncertainty for NOC  
177 measurements in this study, although it is expected to be small.

178  $O_3$  was generated by passing zero air through an  $O_3$  generator (OG-1, PCI Ozone  
179 Corp.) and measured with an  $O_3$  monitor (model 205, 2B Technologies). OH was  
180 produced by photolysis of  $H_2O_2$  (Wang et al., 2010a; Donahue et al., 2012), which was  
181 added by bubbling zero air through a 30 %  $H_2O_2$  solution (Sigma Aldrich). Details  
182 regarding the OH concentration determination and the oxidant levels during these  
183 experiments are described further in the supporting information (SI).  $NH_3$  from a  
184 standard cylinder was added into the chamber through a passivated mass flow controller.  
185  $NH_3$  concentration in the chamber was measured with a Quantum Cascade Laser (QCL,  
186 Aerodyne), whose principle of operation has been described elsewhere (Kosterev et al.,  
187 2002).

188 Unfortunately, the  $NH_3$  background in the dry chamber was consistently at  $\sim 5$

189 ppbv (after cleaning), increasing to a reproducible ~35 ppbv after humidifying to 50 %  
190 RH. While this limited the ability to perform experiments in the complete absence of  
191 ammonia, it did not preclude the derivation of kinetics at the lowest concentration (35  
192 ppbv) and higher attained by further additions of ammonia. In some experiments,  
193 external NH<sub>3</sub> was added to the reactor after ~6 h of reaction to measure the uptake  
194 kinetics of NH<sub>3</sub> by relatively aged SOA. All experiments were conducted at 50±2 %  
195 RH, with zero air provided by an AADCO-737 generator (AADCO Instruments Inc.).

196 The presence of NOC in the SOA particles was also confirmed by Fourier  
197 Transform Infrared (FTIR) Spectroscopy. SOA was collected on a silver membrane  
198 filter (0.2 μm, 47 mm, Sterlitech; stainless steel filter holder), which has a wide IR  
199 window in the range of 650-4000 cm<sup>-1</sup>. A second filter placed behind the first one was  
200 used as a reference sample for IR measurements. The IR spectra were recorded with a  
201 mercury cadmium telluride (MCT) detector at a resolution of 4 cm<sup>-1</sup> for 200 scans in  
202 Diffuse Reflectance Infrared Fourier Transform Spectroscopy (DRIFTS) mode, using  
203 an iS50 spectrometer (Nicolet).

204

## 205 **2.2 Derivation of kinetics.**

206 Reactive uptake coefficients ( $\gamma$ ) of NH<sub>3</sub> to form NOC were calculated based upon  
207 the measured concentration time series of nitrogen atom (N) mass derived from the HR-  
208 ToF-AMS fragment families of C<sub>x</sub>H<sub>y</sub>N<sub>n</sub>, C<sub>x</sub>H<sub>y</sub>ON<sub>n</sub>, C<sub>x</sub>H<sub>y</sub>O<sub>2</sub>N<sub>n</sub>, NH<sub>x</sub> and NO<sub>x</sub> using an  
209 uptake model that has been described in detail previously (Liggio et al., 2005b; Liggio  
210 and Li, 2006a). Briefly, the change in the mass of N (within the NOC) added to a particle

211 exposed to NH<sub>3</sub> as a function of time can be described by,

$$212 \quad \frac{dm_N}{dt} = \gamma_{\text{obs}} \pi a^2 \langle c \rangle c_{\text{NH}_3} F_h \quad (1)$$

213 where  $a$ ,  $\langle c \rangle$  and  $c_{\text{NH}_3}$  are the particle radius, mean molecular speed, and gas-phase  
214 concentration of NH<sub>3</sub>, respectively;  $\gamma_{\text{obs}}$  is the observed uptake coefficient of NH<sub>3</sub> to  
215 form NOC (specifically the N in the NOC);  $F_h$  is a heterogeneous mass factor that  
216 accounts for the loss of hydrogen in ammonia as it reacts heterogeneously to form  
217 particulate phase NOC. We assume  $F_h$  is equal to 0.824 (i.e. N/NH<sub>3</sub>) in this study. From  
218 Eq (1), the N mass as a function of time is given by:

$$219 \quad m_N = \left( \frac{b\pi c_{\text{NH}_3} \langle c \rangle F_h (t-t_0) \gamma_{\text{obs}} + 3(bm_0 + d)^{1/3}}{3b^{1/3}} \right)^3 - \frac{d}{b} \quad (2)$$

220 where,  $b = \frac{3}{4\pi\rho}$ ,  $d = a_0^3$  and are constants. The uptake coefficient ( $\gamma$ ) is derived from  
221 a fit of Eq (2) to the experimental data. Further detail on the derivation and the  
222 parameters used in the fits is given in the SI. It should be pointed out that the NH<sub>x</sub><sup>+</sup>  
223 family (NH<sup>+</sup>, NH<sub>2</sub><sup>+</sup> and NH<sub>3</sub><sup>+</sup>) in the AMS mass spectra may be primarily associated  
224 with inorganic ammonium from the neutralization of the H<sub>2</sub>SO<sub>4</sub> in the seed particle.  
225 However an unknown fraction of the NH<sub>x</sub><sup>+</sup> will arise from the fragmentation of NOC.  
226 For this reason, the uptake coefficients have been derived including and excluding the  
227 N mass of NH<sub>x</sub><sup>+</sup> as upper and lower bounds to  $\gamma$ . The uncertainty in the uptake  
228 coefficient will result from the uncertainty in NOC mass concentration measured by the  
229 AMS, the concentration of NH<sub>3</sub> measured by the QCL and the diameter measured by  
230 the SMPS. In this study, the uncertainty is derived from the uptake model parameters  
231 based on the measured time series of mass concentration of NOC fragments.

232

## 233 3.0 Results and Discussion

### 234 3.1 Identification of NOC

235 A typical mass spectrum of SOA from the ozonolysis of  $\alpha$ -pinene between 4 and 6  
236 hours of reaction in the presence of 40.8 ppbv  $\text{NH}_3$  (Exp. P6) is shown in Figure 1. The  
237 spectrum is dominated by  $\text{C}_x\text{H}_y$  fragments at  $m/z$  27 ( $\text{C}_2\text{H}_3^+$ ), 39 ( $\text{C}_3\text{H}_3^+$ ), 41 ( $\text{C}_3\text{H}_5^+$ )  
238 and 53 ( $\text{C}_4\text{H}_7^+$ );  $\text{C}_x\text{H}_y\text{O}$  fragments at  $m/z$  28 ( $\text{CO}^+$ ), 43 ( $\text{C}_2\text{H}_3\text{O}^+$ ) and 55 ( $\text{C}_3\text{H}_3\text{O}^+$ ); and  
239  $\text{C}_x\text{H}_y\text{O}_2$  fragments at  $m/z$  44 ( $\text{CO}_2^+$ ) and 45 ( $\text{CHO}_2^+$ ). The presence of these fragment  
240 families and the overall mass spectrum is consistent with previously reported mass  
241 spectra of SOA formed from the  $\text{O}_3$  oxidation of  $\alpha$ -pinene at low SOA mass loading  
242 ( $<15 \mu\text{g m}^{-3}$ ) (Shilling et al., 2009).

243 In the presence of  $\text{NH}_3$ , a number of N-containing fragments are also observed.  
244 The mass spectrum containing N-containing fragments only is shown in Figure 1B.  
245 Strong peaks belonging to the  $\text{C}_x\text{H}_y\text{N}_n$  family of fragments dominate the spectrum at  
246  $m/z$  27 ( $\text{CHN}^+$ ), 30 ( $\text{CH}_4\text{N}^+$ ), 42 ( $\text{C}_2\text{H}_4\text{N}^+$ ), 43 ( $\text{C}_2\text{H}_5\text{N}^+$ ), 54 ( $\text{C}_3\text{H}_4\text{N}^+$ ), 55 ( $\text{C}_3\text{H}_5\text{N}^+$ ) and  
247 68 ( $\text{C}_3\text{H}_4\text{N}_2^+$ ,  $\text{C}_4\text{H}_6\text{N}^+$ ). Less prevalent peaks from the  $\text{C}_x\text{H}_y\text{ON}_n$  and  $\text{C}_x\text{H}_y\text{O}_2\text{N}_n$  group  
248 of fragments are also observed at  $m/z$  44 ( $\text{CH}_2\text{ON}^+$ ), 45 ( $\text{CH}_3\text{ON}^+$ ), 58 ( $\text{C}_2\text{H}_4\text{ON}^+$ ), 68  
249 ( $\text{C}_3\text{H}_2\text{ON}^+$ ), 73 ( $\text{C}_2\text{H}_5\text{ON}_2^+$ ,  $\text{C}_3\text{H}_7\text{ON}^+$ ), 86 ( $\text{C}_3\text{H}_6\text{ON}_2^+$ ), 97 ( $\text{C}_4\text{H}_5\text{ON}_2^+$ ), 73  
250 ( $\text{C}_3\text{H}_2\text{O}_2\text{N}^+$ ), 86 ( $\text{C}_2\text{H}_2\text{O}_2\text{N}_2^+$ ), and 91 ( $\text{C}_3\text{H}_9\text{O}_2\text{N}^+$ ). Although the signal intensities of  
251 N-containing fragments are weaker than those of the  $\text{C}_x\text{H}_y$ ,  $\text{C}_x\text{H}_y\text{O}$  and  $\text{C}_x\text{H}_y\text{O}_2$  families,  
252 the results demonstrate that N-containing species are formed. Our results are consistent  
253 with previous work that observed a significant increase in the fraction of organic  
254 constituents with one or two N atoms for  $\text{NH}_3$ -aged  $\alpha$ -pinene SOA (Flores et al., 2014).

255 Similar OA mass spectra were obtained from the OH oxidation ( $\text{H}_2\text{O}_2 + h\nu$ ) of m-  
256 xylene (Figure S3). As shown in Figure S3, the relative intensities of  $\text{C}_x\text{H}_y$ ,  $\text{C}_x\text{H}_y\text{O}$  and  
257  $\text{C}_x\text{H}_y\text{O}_2$  fragment families are slightly different than those of SOA formed via OH  
258 oxidation of m-xylene reported previously (Loza et al., 2012). This is likely due to  
259 differences in experimental reaction conditions such as the oxidant level and mass  
260 loading. The mass spectrum of N-containing fragments for m-xylene derived SOA are  
261 given in Figure S3B, and are also somewhat different than those observed for  $\alpha$ -pinene  
262 derived SOA (Figure 1B). For example, the fragments at  $m/z$  68 ( $\text{C}_3\text{H}_4\text{N}_2^+$ ,  $\text{C}_4\text{H}_6\text{N}^+$  and  
263  $\text{C}_3\text{H}_2\text{ON}^+$ ), 91 ( $\text{C}_3\text{H}_9\text{O}_2\text{N}^+$ ) and 97 ( $\text{C}_4\text{H}_5\text{ON}_2^+$ ) are significantly weaker in the SOA  
264 from m-xylene (Figure S3B) than those from the ozonolysis of  $\alpha$ -pinene (Figure 1B),  
265 suggesting the presence of different types and quantities of the SOA functional groups  
266 required for the organonitrogen forming heterogeneous reactions.

267 The formation of NOC is further confirmed via the IR spectra of the SOA formed  
268 in the presence of  $\text{NH}_3$ . The IR spectra of SOA from the ozonolysis of  $\alpha$ -pinene and the  
269 OH oxidation of m-xylene is shown in Figure 2 and the assignments of the observed IR  
270 bands are summarized in Table S1. After 6 h of ammonia exposure a number of nitrogen  
271 containing bands are tentatively identified. These include,  $\text{NH}_x$  ( $\nu_{\text{as},\text{NH}_2}$ : 3490;  $\nu_{\text{as},\text{NH}_3^+}$ :  
272  $3240\text{ cm}^{-1}$ ;  $\delta_{\text{NH}}$  or  $\nu_{\text{s},\text{CN}}$  1563; and 785 or  $740\text{ cm}^{-1}$ ) and  $\text{C}=\text{N}$  ( $\nu_{\text{s},\text{CN}}$ : 1640;  $\nu_{\text{s},\text{CN}}$ : 1660  
273  $\text{cm}^{-1}$ ) (Nguyen et al., 2013; Lin-Vien et al., 1991) functional groups which are  
274 observable in the SOA from both  $\alpha$ -pinene and m-xylene. The generally small IR  
275 signals associated with the NOC make it difficult to conclusively assign a number of  
276 potential NOC bands particularly since the expected dominant carbonyl and organic

277 acid functional groups associated with SOA are also observed (Table S1).

278 While the above IR assignments are common between experiments using both  
279 VOC precursors, the OH oxidation of m-xylene resulted in a very strong band at 2195  
280  $\text{cm}^{-1}$ , which was not present in the  $\alpha$ -pinene derived SOA (Figure 2) and was potentially  
281 assigned to  $\nu_{\text{s,C=C-C}\equiv\text{N}}$  (Lin-Vien et al., 1991) (a nitrile). At the present time, the exact  
282 formation mechanism leading to this functional group is unknown. However, the double  
283 bond adjacent to the nitrile group suggests that it is unique to the oxidative ring opening  
284 of m-xylene (and likely other aromatics), which is not accessible in the  $\alpha$ -pinene system.  
285 Regardless, the functional groups revealed in the IR absorption spectra supports the  
286 HR-ToF-AMS results and confirms the formation of particle bound NOC.

287

### 288 **3.2 Potential mechanisms contributing to observed NOC**

289 Several mechanisms have been postulated previously with respect to NOC  
290 formation in the presence of ammonia (Zhang et al., 2015). The various mechanisms  
291 generally fall into two categories: reactions of ammonia/ammonium with carbonyl  
292 functional groups in SOA leading to the formation of species with covalently bonded  
293 carbon to nitrogen (Wang et al., 2010b;Zarzana et al., 2012;Yu et al., 2011;Powelson et  
294 al., 2014;Lee et al., 2013a;Trainic et al., 2011;Zhang et al., 2015), or acid-base reactions  
295 between ammonia/ammonium and organic/inorganic acid species in particles leading  
296 to organic ammonium salts (Liu et al., 2012b;Kuwata and Martin, 2012;Zhang et al.,  
297 2015).

298 Several studies have identified the presence of NOC in laboratory generated SOA

299 associated with the presence of carbonyl groups and  $\text{NH}_4^+$  (the dominant form of  $\text{NH}_3$   
300 in particles). For example, using an HR-ToF-AMS, N-containing fragments including  
301 strong ions at  $m/z$  41, 68, 69 and 70 and weak ions at  $m/z$  46, 52, 53, 57, 68 and 96 have  
302 been identified for the uptake of glyoxal on ammonium sulphate particles (Galloway et  
303 al., 2009), attributed to imine and/or imidazole formation. Higher molecular weight N-  
304 containing molecular ions such as  $m/z$  97 ( $\text{C}_4\text{H}_5\text{ON}_2^+$ ), 115 ( $\text{C}_4\text{H}_7\text{O}_2\text{N}_2^+$ ), 129  
305 ( $\text{C}_5\text{H}_9\text{O}_2\text{N}_2^+$ ), 159 ( $\text{C}_6\text{H}_{11}\text{O}_3\text{N}_2^+$ ), 173 ( $\text{C}_7\text{H}_{13}\text{O}_3\text{N}_2^+$ ), 184 ( $\text{C}_7\text{H}_{10}\text{O}_3\text{N}_3^+$ ) have also been  
306 detected using high resolution electrospray ionization mass spectrometry (ESI-MS) for  
307 the same reaction system (Galloway et al., 2009). In addition, SOA, which was formed  
308 through the ozonolysis of  $\alpha$ -pinene and *d*-limonene, subsequently impacted on a  
309 polymeric plate and then exposed to gaseous  $\text{NH}_3$ , resulted in a significant enhancement  
310 in relative abundance of several NOC molecules, such as,  $\text{C}_9\text{H}_{11}\text{NO}_2$ ,  $\text{C}_9\text{H}_{13}\text{NO}_2$ ,  
311  $\text{C}_{19}\text{H}_{29}\text{NO}_4$ ,  $\text{C}_{19}\text{H}_{29}\text{NO}_5$ ,  $\text{C}_{19}\text{H}_{33}\text{NO}_5$  (Laskin et al., 2014).

312 Presently, the gas-phase oxidation mechanism of  $\alpha$ -pinene by ozone has been fairly  
313 well elucidated. In general, the initial step proceeds through cycloaddition of  $\text{O}_3$  to the  
314  $\text{C}=\text{C}$  bond, forming an excited primary ozonide (POZ). The POZ undergoes a  
315 unimolecular isomerization to produce Criegee intermediates (CIs), which  
316 subsequently yield both gas-phase and particle-phase compounds containing hydroxyl,  
317 carbonyl and acidic functional groups (Zhang and Zhang, 2005; Yu et al., 1999). In  
318 particular, previous work has found that organic acids are the dominant SOA component  
319 (Ma et al., 2013). The OH initiated oxidation mechanism of *m*-xylene is more complex  
320 as described by the Master Chemical Mechanism MCM3.1 (Bloss et al., 2005);

321 however it also leads to particle-phase acids and carbonyls (Loza et al., 2012). It has  
322 been found that  $\alpha$ -dicarbonyls are likely the most dominant form of products from the  
323 OH-initiated oxidation of m-xylene (Zhao et al., 2005).

324 Particle-phase carbonyl compounds are present in the current experiments as  
325 confirmed by IR absorption band at  $1725\text{ cm}^{-1}$  (in both systems). The observed HR-  
326 ToF-AMS fragment families of  $\text{C}_x\text{H}_y\text{N}_n$ ,  $\text{C}_x\text{H}_y\text{ON}_n$  and  $\text{C}_x\text{H}_y\text{O}_2\text{N}_n$  indicates that C–N  
327 bonds have formed and they are qualitatively similar to those associated with imine  
328 and/or imidazole formation (Nguyen et al., 2013; Lee et al., 2013a) which is generally  
329 summarized in Scheme S1. The HR-ToF-AMS fragments and the formation of imine  
330 bonds are also consistent with the IR derived functional groups of  $\text{NH}_x$  and C=N  
331 observed in this study (Figure 2; Table S1).

332 Previous studies have observed the neutralization reaction between  $\text{NH}_3$  and  
333 organic acids in both flow reactor (Paciga et al., 2014) and environmental chambers  
334 (Na et al., 2007). In particular, high concentrations of  $\text{NH}_3$  greatly promoted SOA  
335 formation from ozonolysis of  $\alpha$ -pinene (Na et al., 2007). This was ascribed to the  
336 formation of organic ammonium salts. Therefore, the formation of organic ammonium  
337 salts in the current work cannot be entirely discounted. The  $\text{NH}_x$  bands in the IR ( $3490$   
338 and  $3240\text{ cm}^{-1}$ ) as well as the  $\text{NH}_x$  fragments of the HR-ToF-AMS may arise from the  
339 ammonium ion associated with an organic ammonium salt. Although organic acids,  
340 whose IR absorbance bands appear at  $3300\text{-}2500\text{ cm}^{-1}$  for  $\nu_s(\text{OH})$ ,  $1760\text{-}1690\text{ cm}^{-1}$  for  
341  $\nu_s(\text{C=O})$ ,  $1320\text{-}1210\text{ cm}^{-1}$  for  $\nu_s(\text{C-O})$ ,  $1440\text{-}1395$  and  $950\text{-}910\text{ cm}^{-1}$  for  $\delta(\text{OH})$  (Lin-  
342 Vien et al. 1991) were observed, it is likely that the majority of  $\text{NH}_x$  arose from the



343 association with acidic sulfate which may need to be fully neutralized prior to the  
344 formation of organic salts. Regardless, organic salts which primarily contribute to the  
345 AMS derived  $\text{NH}_x$  fragments would not result in fragments containing N, C and O (i.e.  
346  $\text{C}_x\text{H}_y\text{N}_n$ ,  $\text{C}_x\text{H}_y\text{ON}_n$ ,  $\text{C}_x\text{H}_y\text{O}_2\text{N}_n$  and  $\text{NO}_x$ ) which account for the majority of NOC  
347 fragments observed. Finally, the formation of organic ammonium salts is inconsistent  
348 with the observed acidity effect on the uptake coefficients leading to NOC (see Section  
349 3.6).

350 The mechanisms described above intrinsically assume that heterogeneous  
351 reactions occur after the  $\text{NH}_3$  uptake onto the SOA. However, gas-phase reactions  
352 between  $\text{NH}_3$  and gaseous organic carbonyls and/or acids and subsequent condensation  
353 may in principle contribute to the observed particle-phase NOC. Reactions of  
354  $\text{NH}_3/\text{NH}_4^+$  with carbonyls are generally acid catalyzed (Zhang et al., 2015), as shown  
355 in Scheme S1, for both the reaction to form Schiff base and Mannich reaction. This  
356 suggests that if the NOC were gas phase reaction products, a termolecular reaction  
357 would be necessary among carbonyls, acid and  $\text{NH}_3$  in the gas phase; the rates of which  
358 are exceedingly slow. Furthermore, gas-phase reactions leading to particle phase NOC  
359 should be negligible since the calculated reactive uptake coefficients ( $\gamma$ ) of  $\text{NH}_3$  are  
360 positively correlated with particle-phase acidity, and anti-correlated with  $\text{NH}_3$   
361 concentration as will be discussed in Section 3.6. An anti-correlation with the gaseous  
362 reactant is characteristic of heterogeneous reactions (Ma et al., 2010 ). Therefore, as  
363 pointed out in Section 2.2, the uptake coefficients derived including  $\text{NH}_x^+$  should be the  
364 upper bound to  $\gamma$ .

### 365 3.3 Contribution of inorganic and organic NO<sub>y</sub> species to NOC

366 In addition to C<sub>x</sub>H<sub>y</sub>N<sub>n</sub>, C<sub>x</sub>H<sub>y</sub>ON<sub>n</sub> and C<sub>x</sub>H<sub>y</sub>O<sub>2</sub>N<sub>n</sub> fragments as shown in Figures 1  
367 and S3, strong signals from NO<sub>x</sub> (NO<sup>+</sup>; *m/z* 30 and NO<sub>2</sub><sup>+</sup>; *m/z* 46) are also observed in  
368 the particle mass spectra of both VOC systems. These NO<sub>x</sub> fragments may have arisen  
369 from processes other than the uptake of NH<sub>3</sub>. NO<sub>x</sub> fragments in the HR-ToF-AMS  
370 spectra can originate from particle bound NOC, inorganic NO<sub>y</sub> (HNO<sub>3</sub> or NH<sub>4</sub>NO<sub>3</sub>)  
371 and/or organic nitrates possibly formed via the chain termination of RO<sub>2</sub> or RO radicals  
372 by the trace levels of NO or NO<sub>2</sub> in the chamber. Although zero air was used in this  
373 study, trace levels of NO<sub>y</sub> (oxides of nitrogen except N<sub>2</sub>O) were detected in the chamber  
374 as shown in Figure S4. The maximum NO<sub>y</sub> concentration was approximately 0.25 ppbv,  
375 but generally much lower.

376 Figure S5 compares the concentrations of particle-phase NO<sub>x</sub> (NO<sup>+</sup> + NO<sub>2</sub><sup>+</sup>) and  
377 total NOC (T<sub>NOC</sub> = C<sub>x</sub>H<sub>y</sub>N<sub>n</sub> + C<sub>x</sub>H<sub>y</sub>ON<sub>n</sub> + C<sub>x</sub>H<sub>y</sub>O<sub>2</sub>N<sub>n</sub> + NO<sub>x</sub>) in a typical SOA  
378 experiment with a control experiment performed in the absence of α-pinene (0 ppbv).  
379 The NO<sub>x</sub> and T<sub>NOC</sub> concentrations in the control experiment increased only slightly  
380 (from 5.4×10<sup>-17</sup> to 8.4×10<sup>-17</sup> g particle<sup>-1</sup> for T<sub>NOC</sub>) compared to the increases observed  
381 in the presence of VOC (from 7.6×10<sup>-17</sup> to 2.9×10<sup>-16</sup> g particle<sup>-1</sup> for T<sub>NOC</sub>). Assuming  
382 that the increase in T<sub>NOC</sub> in the control experiment was entirely from NO<sub>y</sub>, it would  
383 contribute a maximum of 14 % of the T<sub>NOC</sub> mass measured in the typical SOA  
384 experiment shown in Figure S5. In the control experiment NO<sub>x</sub> fragments accounted  
385 for 74.7±4.9 % of T<sub>NOC</sub>, hence the possible contribution of inorganic NO<sub>y</sub> to T<sub>NOC</sub> mass  
386 in a typical SOA experiment is likely even lower (10.5±0.7) %. This estimation is

387 considered an upper limit to the contributions from inorganic NO<sub>y</sub> species, since 0.4  
388 μg m<sup>-3</sup> of SOA were formed in the control experiment after 6 h of reaction (possibly  
389 from the background air of the chamber), suggesting that a small amount of NOC in  
390 control experiments may also be formed via the uptake of NH<sub>3</sub> by trace amounts of  
391 SOA, which could have contributed at least partially to the NO<sup>+</sup> and NO<sub>2</sub><sup>+</sup> ions in the  
392 particle mass spectrum in the control experiment. It should also be pointed out that the  
393 OH concentration in a typical oxidation experiment here is likely higher than that in the  
394 control experiment, potentially resulting in a higher level of inorganic NO<sub>y</sub>.

395 A further constraint on the contributions of inorganic NO<sub>y</sub> to the HR-ToF-AMS  
396 fragments at *m/z* 30 and *m/z* 46 may be obtained by assuming that all of the measured  
397 gaseous NO<sub>y</sub> is HNO<sub>3</sub> (in a typical SOA experiment). Under this condition, the  
398 solvation of HNO<sub>3</sub> into surface water would contribute to less than 4×10<sup>-21</sup> g particle<sup>-1</sup>  
399 of HNO<sub>3</sub>, calculated using the reported growth factor (*GF*) of SOA from ozonolysis of  
400 α-pinene (1.015 at 50 % RH for 180 nm particle) (Varutbangkul et al., 2006) and the  
401 Henry's law constant of HNO<sub>3</sub> of 2.1 mol kg<sup>-1</sup> Pa<sup>-1</sup> at 298 K (Lelieveld and Crutzen,  
402 1991). This value is significantly lower than the detected particle NO<sub>x</sub> fragment mass  
403 concentration in the current experiments (~10<sup>-17</sup> g particle<sup>-1</sup>) and suggests that the  
404 impact of HNO<sub>3</sub> from the trace level NO<sub>x</sub> in the gas phase during the experiments on  
405 the particle NOC is negligible. In addition, if both NH<sub>3</sub> and NO<sub>x</sub> (ultimately HNO<sub>3</sub>) are  
406 present in the reaction system, then NH<sub>4</sub>NO<sub>3</sub> may be formed (and possibly dissociated  
407 into NH<sub>4</sub><sup>+</sup> and NO<sub>3</sub><sup>-</sup>). Aqueous NH<sub>4</sub>NO<sub>3</sub> (i.e. NH<sub>4</sub><sup>+</sup> and NO<sub>3</sub><sup>-</sup>) can likely be excluded  
408 because the RH (50 %) in this study is lower than the deliquescence RH (DRH, 62%)

409 of  $\text{NH}_4\text{NO}_3$  (Lightstone et al., 2000). Regardless, the characteristic IR bands of  $\text{NO}_3^-$  at  
410 1047, 830, and 713  $\text{cm}^{-1}$  (Wu et al., 2007) , and the strong characteristic IR bands of  
411  $\text{NH}_4\text{NO}_3(\text{s})$  at 1340, 1390 and 1630  $\text{cm}^{-1}$  (Miller and Wilkins, 1952) were not observed  
412 in Figure 2. These results imply that a possible interference by inorganic  $\text{NH}_4\text{NO}_3$  at  
413  $m/z$  30 and 46 is not likely.

414 While inorganic NOy ( $\text{HNO}_3$  &  $\text{NH}_4\text{NO}_3$ ) had little influence on the observed  
415 particle  $\text{NO}^+/\text{NO}_2^+$  fragments (as described above), organic NOy partitioning may also  
416 be possible, leading to NOC that was not derived via the uptake of  $\text{NH}_3$ . In the presence  
417 of NO larger than 10-30 pptv, organonitrates ( $\text{RONO}_2$ ) can be formed through reactions  
418 between organic peroxy radicals ( $\text{RO}_2$ ) and NO (Arey et al., 2001). The initial NO  
419 concentration in these chamber experiments was  $\sim 25$  pptv (Figure S6). The limited  
420 resolution of the FTIR measurements makes it difficult to differentiate between  $\text{RONO}_2$   
421 and other NOC bands ( $\sim 1640, 1315, 870 \text{ cm}^{-1}$ ; Figure 2 and Table S1). However, a  
422 number of observations described below suggest that photo-chemically derived  $\text{RONO}_2$   
423 (hence not NOC from  $\text{NH}_3$ ) was a minor contributor to the observed  $\text{NO}_x$  fragments,  
424 and a further negligible source of  $\text{C}_x\text{H}_y\text{ON}_n$  and  $\text{C}_x\text{H}_y\text{O}_2\text{N}_n$  fragments. Firstly, the photo-  
425 chemical formation of organo-nitrates in various VOC systems is usually associated  
426 with the formation of significantly more  $\text{HNO}_3$  ( $\text{NH}_4\text{NO}_3$  in this study) which was not  
427 observed in the IR measurements here. Secondly, AMS measurements have  
428 demonstrated that the  $\text{NO}^+/\text{NO}_2^+$  ratio specifically for monoterpene derived organo-  
429 nitrates is in the range of 10-15 (Bruns et al., 2010; Fry et al., 2009), in contrast to that  
430 of the current study ( $\sim 2$ ). Thirdly, Farmer et al. (Farmer et al., 2010) have shown that

431  $C_xH_yON_n$  and  $C_xH_yO_2N_n$  fragments from organo-nitrate standards typically account for  
432 <5% of the total N containing mass, in contrast to the current study where they account  
433 for ~30% (Table 2). Finally, there was an observed positive correlation between  
434 particle-phase acidity and the derived uptake coefficients (described in Section 3.6)  
435 based upon these NOC fragments, which is inconsistent with  $RONO_2$  formed photo-  
436 chemically in the gas-phase. Consequently,  $NO_x$ ,  $C_xH_yON_n$  and  $C_xH_yO_2N_n$  fragments  
437 are likely to have arisen primarily from the heterogeneous reactions of  $NH_3$ , and are  
438 thus included in subsequent kinetic calculations.

### 439 **3.4 Contribution of NOC to SOA**

440 The temporal evolution of the four families of N-containing fragments (excluding  
441  $NH_x$ ) and the total SOA during ozonolysis of  $\alpha$ -pinene and OH oxidation of m-xylene  
442 are shown in Figures 3A and 3B, respectively. Note that NOC as defined here is not  
443 likely to be a result of acid-base (organic acid- $NH_3$ ) reactions since  $NH_x$  fragments are  
444 excluded (See section 3.2). The relative contribution of  $T_{NOC}$  to SOA is shown in  
445 Figures 3C and 3D and summarized for all experiments in Table 2. As shown in Figure  
446 3A and B, once the ozonolysis or OH oxidation was initiated all N-containing fragments  
447 increase significantly with time; but their growth rates were much smaller than that for  
448 the bulk of the SOA, as demonstrated by the relatively sharp decline in the  $T_{NOC}/SOA$   
449 of Figures 3C and 3D. Nonetheless, after 6 hours of exposure in these experiments, N-  
450 containing species (based on the quantified HR-ToF-AMS fragments excluding  $NH_x$ )  
451 contributed  $8.9 \pm 1.7$  wt% and  $31.5 \pm 4.4$  wt% (avg over all experiments) of the total SOA  
452 mass from the ozonolysis of  $\alpha$ -pinene and OH oxidation of m-xylene, respectively. As

453 discussed in Section 3.2,  $\alpha$ -dicarbonyls are likely the most dominant products from the  
454 OH-initiated oxidation of m-xylene (Zhao et al., 2005), while organic acids are likely  
455 the dominant SOA components derived from ozonolysis of  $\alpha$ -pinene (Ma et al., 2013).  
456 This is consistent with the higher NOC content in the total SOA mass from the OH  
457 oxidation of m-xylene as shown in Figure 3. After 6 h of reaction, as summarized in  
458 Table 2, the mean N/C ratio is  $0.016 \pm 0.004$  for the ozonolysis of  $\alpha$ -pinene and  
459  $0.065 \pm 0.011$  for the OH oxidation of m-xylene. These N/C ratios are comparable with  
460 that of low-volatility oxidized organic aerosol (OOA, 0.011) and a recently isolated  
461 nitrogen-enriched OA (0.053) (Su, 2011). In a study of the ozonolysis of *d*-limonene by  
462 Laskin et al. (2010), it was found that <6% of the extracted species from fresh SOA  
463 contained an N atom, which was ascribed to reactions with trace amounts of  $\text{NH}_3$  in the  
464 laboratory air or from reactions of dissolved analyte molecules with solvent  
465 (acetonitrile). This value (6 %) is comparable with the  $T_{\text{NOC}}$  content of SOA from the  
466 ozonolysis of  $\alpha$ -pinene in this study (Table 1). In the reactions between glyoxal and  
467 ammonium, N-containing fragments contributed approximately 1 % to the total SOA  
468 mass (Chhabra et al., 2010). The diversity in NOC mass fraction or N/C reported  
469 previously suggests that the N-containing content of SOA will depend upon the  
470 conditions associated with the reaction system, such as the VOC, the oxidant,  $\text{NH}_3$   
471 concentration, mass loading of SOA and the seed particle composition. Regardless, the  
472 relatively large contribution of  $T_{\text{NOC}}$  to the formed SOA here suggests that exposure of  
473 SOA in the atmosphere to ammonia may be an important mechanism leading to ambient  
474 particle phase nitrogen even in the absence of acidic particles (*i.e.* exp P5 here). Note

475 that the above fractional NOC values are probably underestimates, as a fraction of the  
476 measured  $\text{NH}_x$  will also arise from NOC, but is not included in the  $T_{\text{NOC}}$  since the  
477 contribution of inorganic ammonium cannot be differentiated.

478

### 479 **3.5 Contribution of NOC to total nitrogen containing mass:**

480 The relative contribution of each NOC fragment family to the  $T_{\text{NOC}}$  ( $T_{\text{NOC}} = \text{NO}_x$   
481 +  $\text{C}_x\text{H}_y\text{N}_n + \text{C}_x\text{H}_y\text{ON}_n + \text{C}_x\text{H}_y\text{O}_2\text{N}_n$ ), is also shown in Figures 3C and 3D. The above  
482 fragment contribution to  $T_{\text{NOC}}$ , together with the ratio of  $T_{\text{NOC}}$  to the total nitrogen  
483 containing mass ( $\text{TN} = T_{\text{NOC}} + \text{NH}_x$ ) and the  $T_{\text{NOC}}/\text{TN}$  ratio on a nitrogen atom mass  
484 basis ( $N_{\text{NOC}}/N_{\text{TN}}$ ) are summarized for all experiments in Table 2. After 6-hr of  $\text{NH}_3$   
485 exposure (Figure 3C), the ratio of  $\text{NO}_x$ ,  $\text{C}_x\text{H}_y\text{N}_n$ ,  $\text{C}_x\text{H}_y\text{ON}_n$  and  $\text{C}_x\text{H}_y\text{O}_2\text{N}_n$  fragment  
486 families to  $T_{\text{NOC}}$  were 37.2 wt%, 33.5 wt%, 17.0 wt% and 12.2 wt%, respectively for  
487 the ozonolysis of  $\alpha$ -pinene, and 45.6 wt%, 34.3 wt%, 15.7 wt% and 4.5 wt% for the  
488 OH oxidation of m-xylene (Figure 3D). These relative contributions to  $T_{\text{NOC}}$  were  
489 consistent between experiments and VOC systems, with the exception of  $\text{C}_x\text{H}_y\text{O}_2\text{N}_n$   
490 fragments which contributed approximately 3 times less to the  $T_{\text{NOC}}$  in m-xylene  
491 experiments compared to those of  $\alpha$ -pinene (Table 2). Placed in the context of the total  
492 nitrogen containing mass (TN), which includes the inorganic ammonium, NOC formed  
493 from exposure of SOA to  $\text{NH}_3$  accounted for a substantial fraction of the TN (~10-20  
494 wt%) with a generally greater contribution in the m-xylene system under otherwise  
495 similar conditions. However, a better indication of the importance of NOC forming  
496 reactions is derived by computing the above ratio on an atomic nitrogen mass basis

497 ( $N_{\text{NOC}}/N_{\text{TN}}$ ; Table 2). Despite the carbon, hydrogen and oxygen content of the NOC  
498 fragments, the amount of N associated with NOC remains a significant contributor to  
499 the total N mass (~4 – 15 wt%), and is likely underestimated since an unknown fraction  
500 of  $\text{NH}_x$  will be from NOC. Such a high N content in these particles may have  
501 implications for ambient particulate nitrogen loading and subsequent N deposition  
502 which will be discussed further in Section 4.

503

### 504 **3.6 Reaction kinetics.**

505 Typical temporal profiles for  $T_{\text{NOC}}$  during the ozonolysis of  $\alpha$ -pinene, which are  
506 used in the kinetic calculations, can be represented by those for Exp. P3 and P5 (Figure  
507 4). The open circles and solid triangles represent the experimental data, with the fit of  
508 the uptake model shown as red and blue lines during the initial (from 0 to 150 min) and  
509 the final stages (from 400 to 1250 min) of the experiment respectively. In these specific  
510 experiments (P3, P5), the observed initial reactive uptake coefficients of  $\text{NH}_3$  ( $\gamma_{\text{obs,ini}}$ ;  
511 on an atomic N mass basis) to form the N in NOC were  $4.8 \pm 0.2 \times 10^{-3}$  and  $1.07 \pm 0.03 \times 10^{-3}$ ,  
512 respectively. The true uptake coefficients ( $\gamma_{\text{t,ini}}$ ) were obtained by performing gas-  
513 phase diffusion corrections for  $\text{NH}_3$  using a previously reported empirical formula  
514 (Fuchs and Sutugin, 1970; Worsnop et al., 2002; Widmann and Davis, 1997) and the  
515 diffusion coefficient of  $\text{NH}_3$  in air ( $0.1978 \text{ cm}^2 \text{ s}^{-1}$ ) (Massman, 1998). The  
516 corresponding  $\gamma_{\text{t,ini}}$  values for all experiments ranged from  $1.23 \pm 0.04 \times 10^{-3}$  to  
517  $1.52 \pm 0.03 \times 10^{-2}$  (Table 2). As discussed above, a fraction of the observed  $\text{NH}_x$  fragments  
518 are likely to have arisen from NOC. However they are not included in the uptake



519 coefficient estimates of Table 2 and thus results in an underestimate of  $\gamma$ . Conversely,  
520 including  $\text{NH}_x$  in the calculation of  $\gamma$  (Table S2) is considered an overestimate. Despite  
521 this uncertainty, these uptake coefficients on the order of  $10^{-3}$  are relatively large. At  
522 the present time, no data is available for comparison since the uptake kinetics of  $\text{NH}_3$   
523 on organic aerosol has not been reported. However, the uptake coefficients measured in  
524 this study are similar to those observed for glyoxal (Liggio et al., 2005a, b; Liggio and  
525 Li, 2006a), and are 2-4 orders of magnitude higher than biogenic olefins (Liggio and  
526 Li, 2008) and pinonaldehyde (Liggio and Li, 2006a) on acidic surfaces.

527 While not included in the derivation of  $\gamma$  leading to NOC, the  $\text{NH}_x$  data from these  
528 experiments can be used to derive  $\text{NH}_3$  uptake coefficients leading to inorganic  
529 ammonium ( $\gamma_{\text{NH}_4}$ ) using the same approach as above. The resultant  $\gamma_{\text{NH}_4}$  values are  
530 given in Table S2 and range from  $5.3 \times 10^{-4}$  to  $1.78 \times 10^{-2}$  (mean =  $6.4 \times 10^{-3}$ ) comparable  
531 to the range of  $4 \times 10^{-3}$ – $2 \times 10^{-4}$  reported for the competing uptake of  $\text{NH}_3$  with ambient  
532 organic gases by sulfuric acid (Liggio et al., 2011). The current uptake coefficients  
533 leading to  $\text{NH}_4^+$  are similar in magnitude to those leading to NOC, and significantly  
534 less than what would be expected based upon the neutralization of sulfuric acid particle  
535 ( $\sim 0.5 - 1$ ; (Swartz et al., 1999)). These results suggest that under these conditions, the  
536 formation of NOC can compete with the neutralization of acidic particles, possibly due  
537 to kinetic limitations on the uptake of  $\text{NH}_3$  caused by the coating of SOA as has been  
538 demonstrated previously (Liggio et al., 2011).

539

### 540 **3.7 Factors affecting reaction kinetics**

541 To determine the uptake kinetics of  $\text{NH}_3$  by relatively aged SOA during ozonolysis  
542 of  $\alpha$ -pinene or OH oxidation of m-xylene additional ammonia ( $\Delta c$ : ~30 ppbv) was  
543 introduced into the reaction chamber after approximately 6 hr of the original exposure.  
544 As shown in Figure 3A and B, the additional  $\text{NH}_3$  did not result in a change in the  
545 absolute concentration of N-containing species in the SOA. The ratio of TN to SOA  
546 increased slightly in the last half of the experiments, possibly due to the evaporation of  
547 SOA when  $\alpha$ -pinene was entirely consumed or further particle-phase oxidation by  
548 oxidants (OH and/or  $\text{O}_3$ ). A reduced uptake of  $\text{NH}_3$  for the more aged SOA is also  
549 reflected in the derived uptake coefficients from the latter stages of the experiments.  
550 After 400 min of reaction (Figure 4), the NOC uptake had slowed significantly, and the  
551 derived uptake coefficients of  $\text{NH}_3$  to form NOC decreased to  $1.61 \pm 0.24 \times 10^{-5}$  and  
552  $4.01 \pm 0.13 \times 10^{-5}$ , respectively.

553 A number of factors may explain the reduced uptake onto the more aged particles  
554 of these experiments (>400 min; Fig 4). Firstly, this may suggest that in the latter stages  
555 of photochemistry, multi-generational particle-phase products of VOC oxidation  
556 contain functional groups not involved in the NOC forming heterogeneous reactions.  
557 However, the change in the O/C ratio during these experiments was quite small;  
558 increasing to 0.46 from 0.4 over 6 hours (Figure S7). At the same time, precursor VOCs  
559 were not fully depleted after 6 hours, suggesting that carbonyls should continue to be  
560 formed throughout the experiment and not be entirely consumed via a heterogeneous  
561 reaction with  $\text{NH}_3$ . Given that the postulated heterogeneous reactions (Mannich  
562 reaction and/or **reaction to form Schiff base**) are known to be acid catalyzed (Mitsumori

563 et al., 2006), we suggest that a diffusion limitation to the acidic core of the particle (or  
564 to a region where acidity and carbonyls are unavailable) may be responsible for the  
565 slow decrease in uptake with time as significant amount of organic material (e.g., in the  
566 form of SOA) is added to the seed particles. This would have the effect of reducing the  
567 uptake of  $\text{NH}_3$  leading to both NOC and  $\text{NH}_4^+$ , consistent with the derived  $\gamma$  of both. In  
568 particular, the formation of oligomers of high molecular weight (which may be more  
569 likely to hinder liquid phase diffusion) has been noted to occur in various SOA systems  
570 (Kalberer et al., 2004;Gross et al., 2006). This is also consistent with previous  
571 laboratory studies in which a high  $\text{NH}_3$  exposure for several days is required to detect  
572 the BrC in SOA (Nguyen et al., 2013;Lee et al., 2013b;Updyke et al., 2012). The current  
573 results suggest that the formation of NOC from  $\text{NH}_3$  uptake will be more efficient for  
574 newly formed SOA (which is accelerated in the presence of sulfuric acid) compared to  
575 aged SOA.

576 The relationship between  $\gamma_{t,ini}$  and the particle-phase acidity for the ozonolysis of  
577  $\alpha$ -pinene is shown in Figure 5. Since the RH ( $50\pm 2$  %) was lower than the  
578 deliquescence RH (DRH) of the mixtures of  $\text{H}_2\text{SO}_4$ - $\text{Na}_2\text{SO}_4$  used ( $\sim 80$  %), we cannot  
579 reasonably estimate the surface pH with the E-AIM model (Friese and Ebel, 2010),  
580 though it is expected that some surface coverage of water exists. Alternatively, the mole  
581 ratio of  $\text{H}_2\text{SO}_4$  to  $\text{Na}_2\text{SO}_4$  is used as a qualitative metric for the acidity in Figure 5.  
582 Namely, a higher ratio of  $\text{H}_2\text{SO}_4/\text{Na}_2\text{SO}_4$  indicates stronger acidity. As shown in Figure  
583 5, the reactive uptake coefficient for the  $\text{T}_{\text{NOC}}$  ( $\gamma_{t,ini}$ ) increased by approximately a factor  
584 of 4 with increasing particle-phase acidity. This is consistent with the previously

585 postulated acid-catalyzed reaction mechanisms between carbonyls and  $\text{NH}_3$  or  $\text{NH}_4^+$  (in  
586 equilibrium with gas phase  $\text{NH}_3$ ) in Scheme 1 and elsewhere (Nguyen et al.,  
587 2013;Bones et al., 2010). In Figure 5, an upper and lower limit to this qualitative  
588 relationship with acidity is estimated by including and excluding  $\text{NH}_x$  in the derivation  
589 of  $\gamma_{t,\text{ini}}$ , both of which bear the same relationship.

590 Further insight into the controlling factors in this system is also gained from the  
591 relationship between  $\gamma_{t,\text{ini}}$  and gaseous  $\text{NH}_3$ , which is shown in Figures 6, for a fixed  
592 content of particle-phase sulfuric acid ( $\text{H}_2\text{SO}_4/\text{Na}_2\text{SO}_4$  in moles = 1.95). These figures  
593 demonstrate that  $\gamma_{t,\text{ini}}$  for  $\text{T}_{\text{NOC}}$  decreases with increases in  $\text{NH}_3(\text{g})$  concentration  
594 (regardless of the inclusion of  $\text{NH}_x$  into  $\gamma$ ). In other reaction systems, an anti-correlation  
595 between uptake coefficients and gaseous reactant has been used to indicate that  
596 heterogeneous reactions occur on the particle surface, limited by an increasing number  
597 of ineffective collisions between the reactive sites and the gaseous reactant (*i.e.* surface  
598 saturation;(Ma et al., 2010;Pöschl et al., 2001;Mmereki and Donaldson,  
599 2003 ;Kwamena et al., 2004). While this possibility cannot be ruled out here, the above  
600 acidity dependence argues against surface reaction, since a hydrophilic acidic seed is  
601 unlikely to be miscible with a somewhat hydrophobic SOA and thus migrate to the  
602 surface. Rather, we hypothesize that the relationship in Figure 6 is driven by the kinetics  
603 of organic +  $\text{NH}_3/\text{NH}_4^+$  reactions that lead to the NOC. In this scenario, a larger  $\gamma_{t,\text{ini}}$   
604 would be observed at lower  $\text{NH}_3$  concentration when  $\text{NH}_3$  and/or  $\text{NH}_4^+$  in the particle  
605 is rate limiting, and a reduced  $\gamma_{t,\text{ini}}$  at higher  $\text{NH}_3$  (Fig 6) observed when the organic  
606 reactant is the rate limiting reagent in the formation of NOC. This argument is also

607 consistent with a decrease in the  $T_{\text{NOC}}$  fraction of SOA with increasing SOA mass added  
608 as shown in Figure 7, and again suggests that a barrier/diffusion limitation caused by  
609 organic coatings limits the formation of NOC in these experiments. The relatively few  
610 data points of Figure 7 underlie the need for further systematic study to conclusively  
611 determine the controlling factors leading to the formation of NOC.

612

#### 613 **4 Implications**

614 Organonitrogen compounds have been regarded as an important class of brown  
615 carbon in atmospheric particles, and may also have an influence on regional and global  
616 N deposition. As shown in this work, NOC compounds can be formed efficiently and  
617 quickly via the uptake of  $\text{NH}_3$  by newly formed SOA, in contrast to other studies where  
618 NOC forms over several days (Bones et al., 2010). If it is assumed that a steady state  
619 between NOC and SOA is established as observed in this study (i.e. Figures 3 and 4) ,  
620 then a crude estimate of the formation rate of ambient NOC via the uptake of  $\text{NH}_3$  to  
621 biogenic SOA (BSOA) and anthropogenic SOA (ASOA) can be derived. Top-down  
622 estimates of global biogenic BSOA and anthropogenic ASOA formation have been  
623 estimated at approximately 88 and 10 Tg C/yr, respectively (Hallquist et al.,  
624 2009; Farina et al., 2010). Based upon the measured ratio of NOC in SOA (i.e.  $(8.8 \pm 1.7)$   
625 wt% for ozonolysis of  $\alpha$ -pinene and  $(31.5 \pm 4.4)$  wt% for OH oxidation of m-xylene after  
626 6 hours) and a value of 1.4 for OM/OC (Hallquist et al., 2009) the estimated global  
627 NOC via the reactive uptake of  $\text{NH}_3$  are then  $10.8 \pm 2.1$  and  $4.4 \pm 0.6$  Tg/yr from BSOA  
628 and ASOA respectively, given sufficient  $\text{NH}_3$  availability. However, it should be noted

629 that the lowest NH<sub>3</sub> concentration used in this study was significantly higher than that  
630 typically found in the troposphere. While the dependence of the NOC/SOA on NH<sub>3</sub>  
631 concentration was weak in this high concentration regime, it is not clear if it remains so  
632 at more relevant NH<sub>3</sub> levels. In addition, the formation of NOC may not reach a steady  
633 state in the atmosphere, as NH<sub>3</sub>, SOA and acidic sulfate can be present simultaneously,  
634 preventing the formation of an organic barrier as hypothesized in this study. The MAC  
635 of both BSOA and ASOA is known to be enhanced by NH<sub>3</sub> aging (Updyke et al., 2012)  
636 however only to a maximum of  $\sim 0.1 \text{ m}^2 \text{ g}^{-1}$  at 500 nm wavelength. When compared to  
637 black carbon, with a MAC of  $>10 \text{ m}^2 \text{ g}^{-1}$  (Andreae and Gelencser, 2006) and a global  
638 emission of  $\sim 8 \text{ Tg/yr}$  (Bond et al., 2004), the contribution of NOC originating from the  
639 uptake of NH<sub>3</sub> by SOA to light absorption and the overall energy budget is likely to be  
640 small. It should be noted that light absorption by NOC may be relatively more important  
641 in the UV range, where NOC should have a much higher MAC. While this may not  
642 change the energy budget as significantly as black carbon, the actinic flux could be  
643 significantly changed, with different consequences. However, light absorption by NOC  
644 in atmospheric particles may be important regionally where the BC contribution is  
645 minimal.

646       Based upon the mean N/C in SOA after 6 h of reaction ( $1.6 \pm 0.4 \times 10^{-2}$ ;  $\alpha$ -pinene  
647 and  $6.5 \pm 1.1 \times 10^{-2}$ ; m-xylene), the uptake of NH<sub>3</sub> by BSOA and ASOA may contribute  
648 up to  $1.4 \pm 0.4$  and  $0.7 \pm 0.1 \text{ Tg N/yr}$  from the reactive uptake of NH<sub>3</sub>. Although these  
649 values are significantly less than the total global emission of NH<sub>3</sub> ( $33.4 \text{ Tg N/yr}$ ) (Reis  
650 et al., 2009), it may be important on a local or regional scale. The similarity between

651 the uptake coefficients for NOC and inorganic  $\text{NH}_4^+$  suggests that in the presence of  
652 organic coatings, NOC formation can compete with particle neutralization. Furthermore,  
653 under the conditions of these experiments up to 15% of the total N mass is attributed to  
654 NOC. If this value holds true for the ambient atmosphere, then a significant portion of  
655 N in PM is miss-represented as  $\text{NH}_4^+$  or entirely unaccounted for. This will provide a  
656 means to transport more N further from ammonia sources and result in N deposition  
657 patterns poorly predicted by regional models (Cornell et al., 2003;Cape et al., 2011).  
658 Although a more thorough modelling study and further insight into the rates and  
659 mechanisms of NOC formation is required to clearly elucidate its impact on climate  
660 and regional nitrogen deposition, the results of this study suggest that NOC from  $\text{NH}_3$   
661 should be considered with respect to overall deposition of N to sensitive ecosystems.

## 662 **Supporting Information**

663 The Supplement related to this article is available online at.

664

## 665 **Acknowledgements**

666 This research was financially supported by the Clean Air Regulatory Agenda (CARA),  
667 the National Natural Science Foundation of China (41275131) and the Strategic Priority  
668 Research Program of Chinese Academy of Sciences (XDB05040100).

669

## 670 **References:**

671 Aiken, A. C., Peter F. DeCarlo, and Jimenez, J. L.: Elemental analysis of organic species with electron  
672 ionization high-resolution mass spectrometry, *Anal. Chem.*, 79, 8350-8358, doi: 10.1021/ac071150w,  
673 2007.  
674 Alexander, D. T. L., Crozier, P. A., and Anderson, J. R.: Brown carbon spheres in East Asian outflow and

675 their optical properties, *Science*, 321, 833-836, doi: 10.1126/science.1155296, 2008.

676 Andrade-Eiroa, A., Leroy, V., Dagaut, P., and Bedjanian, Y.: Determination of polycyclic aromatic  
677 hydrocarbons in kerosene and bio-kerosene soot, *Chemosphere*, 78, 1342-1349, doi:  
678 10.1016/j.chemosphere.2010.01.005, 2010.

679 Andreae, M. O., and Gelencser, A.: Black carbon or brown carbon? The nature of light-absorbing  
680 carbonaceous aerosols, *Atmos. Chem. Phys.*, 6, 3131-3148, doi: 10.5194/acp-6-3131-2006, 2006.

681 Arey, J., Aschmann, S. M., Kwok, E. S. C., and Atkinson, R.: Alkyl nitrate, hydroxyalkyl nitrate, and  
682 hydroxycarbonyl formation from the nox-air photooxidations of C<sub>5</sub>-C<sub>8</sub> n-alkanes, *J. Phys. Chem. A.*,  
683 105, 1020-1027, doi: 10.1021/jp003292z, 2001.

684 Beddows, D. C. S., Donovan, R. J., Harrison, R. M., Heal, M. R., Kinnersley, R. P., King, M. D.,  
685 Nicholson, D. H., and Thompson, K. C.: Correlations in the chemical composition of rural background  
686 atmospheric aerosol in the UK determined in real time using time-of-flight mass spectrometry *J. Environ.*  
687 *Monit.*, 6 124-133, doi: 10.1039/b311209h 2004.

688 Bloss, C., Wagner, V., Jenkin, M. E., Volkamer, R., Bloss, W. J., Lee, J. D., Heard, D. E., Wirtz, K.,  
689 Martin-Reviejo, M., Rea, G., Wenger, J. C., and Pilling, M. J.: Development of a detailed chemical  
690 mechanism (MCMv3.1) for the atmospheric oxidation of aromatic hydrocarbons, *Atmos. Chem. Phys.*,  
691 5, 641-664, doi: 10.5194/acp-5-641-2005, 2005.

692 Bond, T. C., Streets, D. G., Yarber, K. F., Nelson, S. M., Woo, J.-H., and Klimont, Z.: A technology-  
693 based global inventory of black and organic carbon emissions from combustion, *J. Geogorphy. Res.*, 109,  
694 doi: 10.1029/2003JD003697, 2004.

695 Bond, T. C., Doherty, S. J., Fahey, D. W., Forster, P. M., Berntsen, T., DeAngelo, B. J., Flanner, M. G.,  
696 Ghan, S., Kärcher, B., Koch, D., Kinne, S., Kondo, Y., Quinn, P. K., Sarofim, M. C., Schultz, M. G.,  
697 Schulz, M., Venkataraman, C., Zhang, H., Zhang, S., Bellouin, N., Guttikunda, S. K., Hopke, P. K.,  
698 Jacobson, M. Z., Kaiser, J. W., Klimont, Z., Lohmann, U., Schwarz, J. P., Shindell, D., Storelvmo, T.,  
699 Warren, S. G., and Zender, C. S.: Bounding the role of black carbon in the climate system: A scientific  
700 assessment, *J. Geophys. Res.- Atmos.*, 118, 5380-5552, doi: 10.1002/jgrd.50171, 2013.

701 Bones, D. L., Henricksen, D. K., Mang, S. A., Gonsior, M., Bateman, A. P., Nguyen, T. B., Cooper, W.  
702 J., and Nizkorodov, S. A.: Appearance of strong absorbers and fluorophores in limonene-O<sub>3</sub> secondary  
703 organic aerosol due to NH<sub>4</sub><sup>+</sup>-mediated chemical aging over long time scales, *J. Geophys. Res.- Atmos.*,  
704 115, doi: 10.1029/2009JD012864, 2010.

705 Bruns, E. A., Perraud, V., Zelenyuk, A., Ezell, M. J., Johnson, S. N., Yu, Y., Imre, D., Finlayson-Pitts, B.  
706 J., and Alexander, M. L.: Comparison of ftir and particle mass spectrometry for the measurement of  
707 particulate organic nitrates, *Environ. Sci. Technol.*, 44, 1056-1061, doi: 10.1021/es9029864, 2010.

708 Bunce, N. J., Liu, L., Zhu, J., and Lane, D. A.: Reaction of naphthalene and its derivatives with hydroxyl  
709 radicals in the gas phase, *Environ. Sci. Technol.*, 31, 2252-2259, doi: 10.1021/es960813g, 1997.

710 Bzdek, B. R., Ridge, D. P., and Johnston, M. V.: Amine exchange into ammonium bisulfate and  
711 ammonium nitrate nuclei, *Atmos. Chem. Phys.*, 10, 3495-3503, doi: 10.5194/acp-10-3495-2010, 2010.

712 Cape, J. N., Cornell, S. E., Jickells, T. D., and Nemitz, E.: Organic nitrogen in the atmosphere — Where  
713 does it come from? A review of sources and methods, *Atmos. Res.*, 102, 30-48, doi:  
714 10.1016/j.atmosres.2011.07.009, 2011.

715 Cappa, C. D., Onasch, T. B., Massoli, P., Worsnop, D. R., Bates, T. S., Cross, E. S., Davidovits, P., Hakala,  
716 J., Hayden, K. L., Jobson, B. T., Kolesar, K. R., Lack, D. A., Lerner, B. M., Li, S.-M., Mellon, D.,  
717 Nuaaman, I., Olfert, J. S., Petäjä T., Quinn, P. K., Song, C., Subramanian, R., Williams, E. J., and Zaveri,  
718 R. A.: Radiative absorption enhancements due to the mixing state of atmospheric black carbon, *Science*,



719 337, 1078-1081, doi: 10.1126/science.1223447, 2012.

720 Chan, L. P., and Chan, C. K.: Displacement of ammonium from aerosol particles by uptake of  
721 triethylamine, *Aerosol Sci. Technol.*, 46, 236-247, doi: 10.1080/02786826.2011.618815, 2012.

722 Cheng, Y., Li, S.-M., and Leithead, A.: Chemical characteristics and origins of nitrogen-containing  
723 organic compounds in PM<sub>2.5</sub> aerosols in the lower fraser valley, *Environ. Sci. Technol.*, 40, 5846-5852,  
724 doi: 10.1021/es0603857, 2006.

725 Chhabra, P. S., Flagan, R. C., and Seinfeld, J. H.: Elemental analysis of chamber organic aerosol using  
726 an aerodyne high-resolution aerosol mass spectrometer, *Atmos. Chem. Phys.*, 10, 4111-4131, doi:  
727 10.5194/acp-10-4111-2010, 2010.

728 Cornell, S. E., Jickells, T. D., Cape, J. N., Rowland, A. P., and Duce, R. A.: Organic nitrogen deposition  
729 on land and coastal environments: a review of methods and data, *Atmos. Environ.*, 37, 2173-2191, doi:  
730 10.1016/S1352-2310(03)00133-X, 2003.

731 Darer, A. I., Cole-Filipiak, N. C., O'Connor, A. E., and Elrod, M. J.: Formation and stability of  
732 atmospherically relevant isoprene-derived organosulfates and organonitrates, *Environ. Sci. Technol.*, 45,  
733 1895-1902, doi: 10.1021/es103797z, 2011.

734 DeCarlo, P. F., Kimmel, J. R., Trimborn, A., Northway, M. J., Jayne, J. T., Aiken, A. C., Gonin, M.,  
735 Fuhrer, K., Horvath, T., Docherty, K. S., Worsnop, D. R., and Jimenez, J. L.: Field-deployable, high-  
736 resolution, time-of-flight aerosol mass spectrometer, *Anal. Chem.*, 78, 8281-8289, doi:  
737 10.1021/ac061249n, 2006.

738 Donahue, N. M., Henry, K. M., Mentel, T. F., Kiendler-Scharr, A., Spindler, C., Bohn, B., Brauers, T.,  
739 Dorn, H. P., Fuchs, H., Tillmann, R., Wahner, A., Saathoff, H., Naumann, K.-H., Möhler, O., Leisner, T.,  
740 Müller, L., Reinnig, M.-C., Hoffmann, T., Salo, K., Hallquist, M., Frosch, M., Bilde, M., Tritscher, T.,  
741 Barmet, P., Praplan, A. P., DeCarlo, P. F., Dommen, J., Prévôt, A. S. H., and Baltensperger, U.: Aging of  
742 biogenic secondary organic aerosol via gas-phase OH radical reactions, *Proc. Natl. Acad. Sci. USA*, 109  
743 13503-13508, doi: 10.1073/pnas.1115186109, 2012.

744 Farina, S. C., Adams, P. J., and Pandis, S. N.: Modeling global secondary organic aerosol formation and  
745 processing with the volatility basis set: Implications for anthropogenic secondary organic aerosol, *J.*  
746 *Geophys. Res.- Atmos.*, 115, D09202, doi: 10.1029/2009JD013046, 2010.

747 Farmer, D. K., Matsunaga, A., Docherty, K. S., Surratt, J. D., Seinfeld, J. H., Ziemann, P. J., and Jimenez,  
748 J. L.: Response of an aerosol mass spectrometer to organonitrates and organosulfates and implications  
749 for atmospheric chemistry, *Proc. Natl. Acad. Sci. USA*, 107, 6670-6675, doi: 10.1073/pnas.0912340107,  
750 2010.

751 Flores, J. M., Washenfelder, R. A., Adler, G., Lee, H. J., Segev, L., Laskin, J., Laskin, A., Nizkorodov, S.  
752 A., Brown, S. S., and Rudich, Y.: Complex refractive indices in the near-ultraviolet spectral region of  
753 biogenic secondary organic aerosol aged with ammonia, *Phys. Chem. Chem. Phys.*, 16, 10629-10642,  
754 10.1039/C4CP01009D, 2014.

755 Friese, E., and Ebel, A.: Temperature dependent thermodynamic model of the system  
756  $H^+-NH_4^+-Na^+-SO_4^{2-}-NO_3^- -Cl^- -H_2O$ , *J. Phys. Chem. A.*, 114, 11595-11631, doi: 10.1021/jp101041j,  
757 2010.

758 Fry, J. L., Kiendler-Scharr, A., Rollins, A. W., Wooldridge, P. J., Brown, S. S., Fuchs, H., Dubé W.,  
759 Mensah, A., dal Maso, M., Tillmann, R., Dorn, H. P., Brauers, T., and Cohen, R. C.: Organic nitrate and  
760 secondary organic aerosol yield from NO<sub>3</sub> oxidation of β-pinene evaluated using a gas-phase  
761 kinetics/aerosol partitioning model, *Atmos. Chem. Phys.*, 9, 1431-1449, doi: 10.5194/acp-9-1431-2009,  
762 2009.

763 Fuchs, N. A., and Sutugin, A. G.: Highly dispersed aerosols, Butterworth-Heinemann, Newton, MA, 1970.

764 Galloway, M. M., Chhabra, P. S., Chan, A. W. H., Surratt, J. D., Flagan, R. C., Seinfeld, J. H., and Keutsch,

765 F. N.: Glyoxal uptake on ammonium sulphate seed aerosol: reaction products and reversibility of uptake

766 under dark and irradiated conditions, *Atmos. Chem. Phys.*, 9, 3331-3345, doi: 10.5194/acp-9-3331-2009,

767 2009.

768 Garca-Gomez, H., Garrido, J. L., Vivanco, M. G., Lassaletta, L., Rabago, I., Avila, A., Tsyro, S., Sanchez,

769 G., Gonzalez Ortiz, A., Gonzalez-Fernandez, I., and Alonso, R.: Nitrogen deposition in Spain: Modeled

770 patterns and threatened habitats within the Natura 2000 network, *Sci. Total Environ.*, 485-486, 450-460,

771 doi: 10.1016/j.scitotenv.2014.03.112, 2014.

772 Gross, D. S., Galli, M. E., Kalberer, M., Prevot, A. S. H., Dommen, J., Alfarra, M. R., Duplissy, J.,

773 Gaeggeler, K., Gascho, A., Metzger, A., and Baltensperger, U.: Real-time measurement of oligomeric

774 species in secondary organic aerosol with the aerosol time-of-flight mass spectrometer, *Anal. Chem.*, 78,

775 2130-2137, doi: 10.1021/ac060138l, 2006.

776 Hallquist, M., C.Wenger, J., Baltensperger, U., Rudich, Y., Simpson, D., Claeys, M., Dommen, J.,

777 Donahue, N. M., George, C., Goldstein, A. H., Hamilton, J. F., Herrmann, H., Hoffmann, T., Iinuma, Y.,

778 Jang, M., Jenkin, M. E., Jimenez, J. L., Kiendler-Scharr, A., Maenhaut, W., McFiggans, G., Mentel, T.

779 F., Monod, A., Prevot, A. S. H., Seinfeld, J. H., Surratt, J. D., Szmigielski, R., and Wildt, J.: The

780 formation, properties and impact of secondary organic aerosol: current and emerging issues, *Atmos.*

781 *Chem. Phys.*, 9, 5155-5236, doi: 10.5194/acp-9-5155-2009, 2009.

782 Hawkins, L. N., Russell, L. M., Covert, D. S., Quinn, P. K., and Bates, T. S.: Carboxylic acids, sulfates,

783 and organosulfates in processed continental organic aerosol over the southeast Pacific Ocean during

784 VOCALS-REx 2008, *J. Geophys. Res. - Atmos.*, 115, D13201

785 doi: 10.1029/2009jd013276, 2010.

786 Heald, C. L., J. L. Collett, J., Lee, T., Benedict, K. B., Schwandner, F. M., Li, Y., Clarisse, L., Hurtmans,

787 D. R., Van Damme, M., Clerbaux, C., Coheur, P. F., Philip, S., Martin, R. V., and Pye, H. O. T.:

788 Atmospheric ammonia and particulate inorganic nitrogen over the United States, *Atmos. Chem. Phys.*,

789 12, 10295-10312, doi: 10.5194/acp-12-10295-2012, 2012.

790 Iinuma, Y., Ge, O. B., Kahnt, A., and Herrmann, H.: Laboratory chamber studies on the formation of

791 organosulfates from reactive uptake of monoterpene oxides, *Phys. Chem. Chem. Phys.*, , 11, 7985-7997,

792 doi: 10.1039/b904025k, 2009.

793 Kalberer, M., Paulsen, D., Sax, M., Steinbacher, M., Dommen, J., Prevot, A. S. H., Fisseha, R.,

794 Weingartner, E., Frankevich, V., Zenobi, R., and Baltensperger, U.: Identification of polymers as major

795 components of atmospheric organic aerosols, *Science*, 303, 1659-1662, doi: 10.1126/science.1092185,

796 2004.

797 Kinsey, J. S., Hays, M. D., Dong, Y., Williams, D. C., and Logan, R.: Chemical characterization of the

798 fine particle emissions from commercial aircraft engines during the Aircraft Particle Emissions

799 Experiment (APEX) 1 to 3, *Environ. Sci. Technol.*, 45, 3415-3421, doi: 10.2514/1.36371, 2011.

800 Kosterev, A. A., Curl, R. F., Tittel, F. K., Kohler, R., Gmachl, C., Capasso, F., Sivco, D. L., and Cho, A.

801 Y.: Transportable automated ammonia sensor based on a pulsed thermoelectrically cooled quantum-

802 cascade distributed feedback laser, *Appl. Optics*, 41, 573-578, doi: 10.1364/ao.41.000573, 2002.

803 Kourchev, I., O'Connor, I. P., Giorio, C., Fuller, S. J., Kristensen, K., Maenhaut, W., Wenger, J. C.,

804 Sodeau, J. R., Glasius, M., and Kalberer, M.: Effects of anthropogenic emissions on the molecular

805 composition of urban organic aerosols: An ultrahigh resolution mass spectrometry study, *Atmos.*

806 *Environ.*, 89, 525-532, doi: 10.1016/j.atmosenv.2014.02.051, 2014.

807 Kuwata, M., and Martin, S. T.: Phase of atmospheric secondary organic material affects its reactivity,  
808 Proc. Nat. Acad. Sci. USA, 109, 17354-17359, doi: 10.1073/pnas.12090711109, 2012.

809 Kwamena, N.-O. A., Thornton, J. A., and Abbatt, J. P. D.: Kinetics of surface-bound benzo[a]pyrene and  
810 ozone on solid organic and salt aerosols, J. Phys. Chem. A., 108, 11626-11634, doi: 10.1021/jp046161x,  
811 2004.

812 Laskin, A., Laskin, J., and Nizkorodov, S. A.: Chemistry of atmospheric brown carbon, chemical reviews,  
813 115, 4335-4382, 10.1021/cr5006167, 2015.

814 Laskin, J., Laskin, A., Roach, P. J., Slysz, G. W., Anderson, G. A., Nizkorodov, S. A., Bones, D. L., and  
815 Nguyen, L. Q.: High-resolution desorption electrospray ionization mass spectrometry for chemical  
816 characterization of organic aerosols, Anal. Chem., 82, 2048-2058, doi: 10.1021/ac902801f, 2010.

817 Laskin, J., Laskin, A., Nizkorodov, S. A., Roach, P., Eckert, P., Gilles, M. K., Wang, B., Lee, H. J., and  
818 Hu, Q.: Molecular selectivity of brown carbon chromophores, Environ. Sci. Technol., 48, 12047-12055,  
819 10.1021/es503432r, 2014.

820 Lee, A. K. Y., Zhao, R., Li, R., Liggio, J., Li, S.-M., and Abbatt, J. P. D.: Formation of light absorbing  
821 organo-nitrogen species from evaporation of droplets containing glyoxal and ammonium sulfate, Environ.  
822 Sci. Technol., 47, 12819-12826, doi: 10.1021/es402687w, 2013a.

823 Lee, H. J., Laskin, A., Laskin, J., and Nizkorodov, S. A.: Excitation emission spectra and fluorescence  
824 quantum yields for fresh and aged biogenic secondary organic aerosols, Environ. Sci. Technol., 47, 5763-  
825 5770, doi: 10.1021/es400644c, 2013b.

826 Lee, H. J., Aiona, P. K., Laskin, A., Laskin, J., and Nizkorodov, S. A.: Effect of solar radiation on the  
827 optical properties and molecular composition of laboratory proxies of atmospheric brown carbon,  
828 Environ. Sci. Technol., 48, 10217-10226, 10.1021/es502515r, 2014.

829 Lelieveld, J., and Crutzen, P. J.: The role of clouds in tropospheric photochemistry, J. Atmos. Chem., 12,  
830 229-267, doi: 10.1007/BF00048075, 1991.

831 Liggio, J., Li, S. M., and McLaren, R.: Heterogeneous reactions of glyoxal on particulate matter:  
832 Identification of acetals and sulfate esters, Environ. Sci. Technol., 39, 1532-1541, doi:  
833 10.1021/es048375y, 2005a.

834 Liggio, J., Li, S. M., and McLaren, R.: Reactive uptake of glyoxal by particulate matter, J. Geophys.  
835 Res.- Atmos., 110, D10304, doi: 10.1029/2004jd005113, 2005b.

836 Liggio, J., and Li, S. M.: Reactive uptake of pinonaldehyde on acidic aerosols, J. Geophys. Res.- Atmos.,  
837 111, D24303, doi:10.1029/2005jd006978, doi: 10.1029/2005JD006978, 2006a.

838 Liggio, J., and Li, S. M.: Organosulfate formation during the uptake of pinonaldehyde on acidic sulfate  
839 aerosols, Geophys. Res. Lett., 33, doi: 10.1029/2006GL026079, 2006b.

840 Liggio, J., and Li, S. M.: Reversible and irreversible processing of biogenic olefins on acidic aerosols,  
841 Atmos. Chem. Phys., 8, 2039-2055, doi: 10.5194/acp-8-2039-2008, 2008.

842 Liggio, J., Li, S.-M., Vlasenko, A., Stroud, C., and Makar, P.: Depression of ammonia uptake to sulfuric  
843 acid aerosols by competing uptake of ambient organic gases, Environ. Sci. Technol., 45, 2790-2796, doi:  
844 10.1021/es103801g, 2011.

845 Lightstone, J. M., Onasch, T. B., Imre, D., and Oatis, S.: Deliquescence, efflorescence, and water activity  
846 in ammonium nitrate and mixed ammonium nitrate/succinic acid microparticles, J. Phys. Chem. A., 104,  
847 9337-9346, doi: 10.1021/jp002137h, 2000.

848 Lin-Vien, D., Colthup, N. B., Fateley, W. G., and Grasselli, J. G.: The handbook of infrared and raman  
849 characteristic frequencies of organic molecules, A Division of Harcourt Brace & Company 525 B Street,  
850 Suite 1900, San Diego, California 92101-4495, 1991.

851 Liu, X., Zhang, Y., Han, W., Tang, A., Shen, J., Cui, Z., Vitousek, P., Erisman, J. W., Goulding, K.,  
852 Christie, P., Fangmeier, A., and Zhang, F.: Enhanced nitrogen deposition over China, *Nature*, 494, 459-  
853 462, [http://www.nature.com/nature/journal/v494/n7438/abs/nature11917.html#supplementary-](http://www.nature.com/nature/journal/v494/n7438/abs/nature11917.html#supplementary-information)  
854 [information](http://www.nature.com/nature/journal/v494/n7438/abs/nature11917.html#supplementary-information), 2013.

855 Liu, Y., Han, C., Liu, C., Ma, J., Ma, Q., and He, H.: Differences in the reactivity of ammonium salts  
856 with methylamine, *Atmos. Chem. Phys.*, 12, 4855-4865, doi: 10.5194/acp-12-4855-2012, 2012a.

857 Liu, Y., Ma, Q., and He, H.: Heterogeneous uptake of amines by citric acid and humic acid, *Environ. Sci*  
858 *Technol.*, 46, 11112-11118, doi: 10.1021/es302414v, 2012b.

859 Loza, C. L., Chhabra, P. S., Yee, L. D., Craven, J. S., Flagan, R. C., and Seinfeld, J. H.: Chemical aging  
860 of m-xylene secondary organic aerosol: Laboratory chamber study, *Atmos. Chem. Phys.*, 12, 151-167,  
861 doi: 10.5194/acp-12-151-2012, 2012.

862 Ma, J., Liu, Y., and He, H.: Degradation kinetics of anthracene by ozone on mineral oxides, *Atmos.*  
863 *Environ.*, 44, 4446-4453, doi: 10.1016/j.atmosenv.2010.07.042, 2010

864 Ma, Y., Brooks, S. D., Vidaurre, G., Khalizov, A. F., Wang, L., and Zhang, R.: Rapid modification of  
865 cloud-nucleating ability of aerosols by biogenic emissions, *Geophys. Res. Lett.*, 40, 6293-6297,  
866 doi:10.1002/2013GL057895, 2013.

867 Massman, W. J.: A Review of the molecular diffusivities of H<sub>2</sub>O, CO<sub>2</sub>, CH<sub>4</sub>, CO, O<sub>3</sub>, SO<sub>2</sub>, NH<sub>3</sub>, N<sub>2</sub>O,  
868 NO, AND NO<sub>2</sub> in air, O<sub>2</sub> and N<sub>2</sub> near STP, *Atmos. Environ.*, 32, 1111-1127, doi: 10.1016/S1352-  
869 2310(97)00391-9, 1998.

870 Miller, F. A., and Wilkins, C. H.: Infrared spectra and characteristic frequencies of inorganic ions, *Anal.*  
871 *Chem.*, 24, 1253-1294, doi: 10.1021/ac60068a007, 1952.

872 Mitsumori, S., Zhang, H., Cheong, P. H. Y., Houk, K. N., Tanaka, F., and Barbas, C. F.: Direct asymmetric  
873 anti-Mannich-Type reactions catalyzed by a designed amino acid, *J. Am. Chem. Soc.*, 128, 1040-1041,  
874 doi: 10.1021/ja056984f, 2006.

875 Mmereki, B. T., and Donaldson, D. J.: Direct observation of the kinetics of an atmospherically important  
876 reaction at the air-aqueous interface, *J. Phys. Chem. A*, 107 11038-11042, doi: 10.1021/jp036119m,  
877 2003

878 Moise, T., Flores, J. M., and Rudich, Y.: Optical properties of secondary organic aerosols and their  
879 changes by chemical processes, *Chemical Reviews*, 115, 4400-4439, 10.1021/cr5005259, 2015.

880 Na, K., Song, C., Switzer, C., and Cocker, D. R.: Effect of ammonia on secondary organic aerosol  
881 formation from  $\alpha$ -pinene ozonolysis in dry and humid conditions, *Environ. Sci. Technol.*, 41, 6096-6102,  
882 10.1021/es061956y, 2007.

883 Nguyen, Q. T., Kristensen, T. B., Hansen, A. M. K., Skov, H., Bossi, R., Massling, A., Sorensen, L. L.,  
884 Bilde, M., Glasius, M., and Nojgaard, J. K.: Characterization of humic-like substances in Arctic aerosols,  
885 *J. Geophys. Res.- Atmos.*, 119, 5011-5027, doi: 10.1002/2013jd020144, 2014.

886 Nguyen, T. B., Lee, P. B., Updyke, K. M., Bones, D. L., Laskin, J., Laskin, A., and Nizkorodov, S. A.:  
887 Formation of nitrogen- and sulfur-containing light-absorbing compounds accelerated by evaporation of  
888 water from secondary organic aerosols, *J. Geophys. Res.- Atmos.*, 117, D01207, doi:  
889 10.1029/2011JD016944, 2012.

890 Nguyen, T. B., Laskin, A., Laskin, J., and Nizkorodov, S. A.: Brown carbon formation from  
891 ketoaldehydes of biogenic monoterpenes, *Faraday Discuss.*, 165, 473-494, doi: 10.1039/C3FD00036B,  
892 2013.

893 Paciga, A. L., Riipinen, I., and Pandis, S. N.: Effect of Ammonia on the Volatility of Organic Diacids,  
894 *Environ. Sci. Technol.*, 48, 13769-13775, 10.1021/es5037805, 2014.

895 Pöschl, U., Letzel, T., Schauer, C., and Niessner, R.: Interaction of ozone and water vapor with spark  
896 discharge soot aerosol particles coated with benzo[a]pyrene: O<sub>3</sub> and H<sub>2</sub>O adsorption, benzo[a]pyrene  
897 degradation, and atmospheric implications, *J. Phys. Chem. A*, 105, 4029-4041, doi: 10.1021/jp004137n,  
898 2001.

899 Powelson, M. H., Espelien, B. M., Hawkins, L. N., Galloway, M. M., and Haan, D. O. D.: Brown carbon  
900 formation by aqueous-phase carbonyl compound reactions with amines and ammonium sulfate, *Environ.*  
901 *Sci. Technol.*, 48, 985-993, doi: 10.1021/es4038325, 2014.

902 Qiu, C., Wang, L., Lal, V., Khalizov, A. F., and Zhang, R.: Heterogeneous reactions of alkylamines with  
903 ammonium sulfate and ammonium bisulfate, *Environ. Sci. Technol.*, 45, 4748-4755, doi:  
904 10.1021/es1043112, 2011.

905 Reis, S., Pinder, R. W., Zhang, M., Lijie, G., and Sutton, M. A.: Reactive nitrogen in atmospheric  
906 emission inventories, *Atmos. Chem. Phys.*, 9, 7657-7677, doi: 10.5194/acp-9-7657-2009, 2009.

907 Russell, L. M., Bahadur, R., and Ziemann, P. J.: Identifying organic aerosol sources by comparing  
908 functional group composition in chamber and atmospheric particles, *Proc. Natl. Acad. Sci. USA*, 108,  
909 3516–3521, doi: 10.1073/pnas.1006461108, 2011.

910 Saleh, R., Hennigan, C. J., McMeeking, G. R., Chuang, W. K., Robinson, E. S., Coe, H., Donahue, N.  
911 M., and Robinson, A. L.: Absorptivity of brown carbon in fresh and photo-chemically aged biomass-  
912 burning emissions, *Atmos. Chem. Phys.*, 13, 7683-7693, doi: 10.5194/acp-13-7683-2013, 2013.

913 Salma, I., Mészáros, T., Maenhaut, W., Vass, E., and Majer, Z.: Chirality and the origin of atmospheric  
914 humic-like substances, *Atmos. Chem. Phys.*, 10, 1315-1327, doi: 10.5194/acp-10-1315-2010, 2010.

915 Sareen, N., Moussa, S. G., and McNeill, V. F.: Photochemical aging of light-absorbing secondary organic  
916 aerosol material, *J. Phys. Chem. A*, 117, 2987-2996, 2013.

917 Shilling, J. E., Chen, Q., King, S. M., Rosenoern, T., Kroll, J. H., Worsnop, D. R., DeCarlo, P. F., Aiken,  
918 A. C., Sueper, D., Jimenez, J. L., and Martin, S. T.: Loading-dependent elemental composition of  $\alpha$ -  
919 pinene SOA particles, *Atmos. Chem. Phys.*, 9, 771-782, doi: 10.5194/acp-9-771-2009, 2009.

920 Souza, K. F., Carvalho, L. R. F., Allen, A. G., and Cardoso, A. A.: Diurnal and nocturnal measurements  
921 of PAH, nitro-PAH, and oxy-PAH compounds in atmospheric particulate matter of a sugar cane burning  
922 region, *Atmos. Environ.*, 83, 193-201, doi: 10.1016/j.atmosenv.2013.11.007, 2014.

923 Stocker, T. F., Qin, D., Plattner, G.-K., Tignor, M. M. B., Allen, S. K., Boschung, J., Nauels, A., Xia, Y.,  
924 Bex, V., and Midgley, P. M.: Climate change 2013 the physical science basis, Intergovernmental Panel  
925 on Climate Change, Switzerland, 33, 2013.

926 Su, Y. L.: Characterization of the sources and processes of organic and inorganic aerosols in New York  
927 City with a high-resolution time-of flight aerosol mass spectrometer, *Atmos. Chem. Phys.*, 11, 1581-  
928 1602, doi: 10.5194/acp-11-1581-2011, 2011.

929 Surratt, J. D., Kroll, J. H., Kleindienst, T. E., Edney, E. O., Claeys, M., Sorooshian, A., Ng, N. L.,  
930 Offenberg, J. H., Lewandowski, M., Jaoui, M., Flagan, R. C., and Seinfeld, J. H.: Evidence for  
931 organosulfates in secondary organic aerosol, *Environ. Sci. Technol.*, 41, 517-527, doi:  
932 10.1021/es062081q, 2006.

933 Swartz, E., Shi, Q., Davidovits, P., Jayne, J. T., Worsnop, D. R., and Kolb, C. E.: Uptake of gas-phase  
934 ammonia. 2. uptake by sulfuric acid surfaces, *J. Phys. Chem. A*, 103, 8824-8833, doi:  
935 10.1021/jp991697h, 1999.

936 Trainic, M., Riziq, A. A., Lavi, A., Flores, J. M., and Rudich, Y.: The optical, physical and chemical  
937 properties of the products of glyoxal uptake on ammonium sulfate seed aerosols, *Atmos. Chem. Phys.*,  
938 11, 9697-9707, doi: 10.5194/acp-11-9697-2011, 2011.

939 Updyke, K. M., Nguyen, T. B., and Nizkorodov, S. A.: Formation of brown carbon via reactions of  
940 ammonia with secondary organic aerosols from biogenic and anthropogenic precursors, *Atmos. Environ.*,  
941 63, 22-31, doi: 10.1016/j.atmosenv.2012.09.012, 2012.

942 Varutbangkul, V., Brechtel, F. J., Bahreini, R., Ng, N. L., Keywood, M. D., Kroll, J. H., Flagan, R. C.,  
943 Seinfeld, J. H., Lee, A., and Goldstein, A. H.: Hygroscopicity of secondary organic aerosols formed by  
944 oxidation of cycloalkenes, monoterpenes, sesquiterpenes, and related compounds, *Atmos. Chem. Phys.*,  
945 6, 2367-2388, doi: 10.5194/acp-6-2367-2006, 2006.

946 Wang, K., Ge, M., and Wang, W.: Kinetics of the gas-phase reactions of 5-hexen-2-one with OH and  
947 NO<sub>3</sub> radicals and O<sub>3</sub>, *Chem. Phys. Lett.*, 490, 29-33, doi: 10.1016/j.cplett.2010.03.023, 2010a.

948 Wang, X. F., Gao, S., Yang, X., Chen, H., Chen, J. M., Zhuang, G. S., Surratt, J. D., Chan, M. N., and  
949 Seinfeld, J. H.: Evidence for high molecular weight nitrogen-containing organic salts in urban aerosols,  
950 *Environ. Sci. Technol.*, 44, 4441-4446, doi: 10.1021/es1001117, 2010b.

951 Widmann, J. F., and Davis, E. J.: Mathematical models of the uptake of ClONO<sub>2</sub> and other gases by  
952 atmospheric aerosols, *J. Aerosol Sci.*, 28, 87-106, doi: 10.1016/S0021-8502(96)00060-2, 1997.

953 Worsnop, D. R., Morris, J. W., Shi, Q., Davidovits, P., and Kolb, C. E.: A chemical kinetic model for  
954 reactive transformations of aerosol particles, *Geophys. Res. Lett.*, 29, 1996, doi: 10.1029/2002gl015542,  
955 2002.

956 Wu, H. B., Chan, M. N., and Chan, C. K.: FTIR characterization of polymorphic transformation of  
957 ammonium nitrate, *Aerosol Sci. Technol.*, 41, 581-588, doi: 10.1080/02786820701272038, 2007.

958 Yu, G., Bayer, A. R., Galloway, M. M., Korshavn, K. J., Fry, C. G., and Keutsch, F. N.: Glyoxal in  
959 aqueous ammonium sulfate solutions: Products, kinetics and hydration effects, *Environ. Sci. Technol.*,  
960 45, 6336-6342, doi: 10.1021/es200989n, 2011.

961 Yu, J., Cocker, D., III, Griffin, R., Flagan, R., and Seinfeld, J.: Gas-phase ozone oxidation of  
962 monoterpenes: gaseous and particulate products, *J. Atmos. Chem.*, 34, 207-258, doi:  
963 10.1023/a:1006254930583, 1999.

964 Zarzana, K. J., De Haan, D. O., Freedman, M. A., Hasenkopf, C. A., and Tolbert, M. A.: Optical  
965 properties of the products of  $\alpha$ -dicarbonyl and amine reactions in simulated cloud droplets, *Environ. Sci.*  
966 *Technol.*, 46, 4845-4851, doi: 10.1021/es2040152, 2012.

967 Zhang, D., and Zhang, R.: Ozonolysis of  $\alpha$ -pinene and  $\beta$ -pinene: Kinetics and mechanism, *J. Chem. Phys.*,  
968 122, 114308-114318, doi: 10.1063/1.1862616g, 2005.

969 Zhang, R., Wang, G., Guo, S., Zamora, M. L., Ying, Q., Lin, Y., Wang, W., Hu, M., and Wang, Y.:  
970 Formation of urban fine particulate matter, *Chemical Reviews*, 115, 3803-3855,  
971 10.1021/acs.chemrev.5b00067, 2015.

972 Zhao, J., Zhang, R., Misawa, K., and Shibuya, K.: Experimental product study of the OH-initiated  
973 oxidation of m-xylene, *Journal of Photochemistry and Photobiology A: Chemistry*, 176, 199-207,  
974 <http://dx.doi.org/10.1016/j.jphotochem.2005.07.013>, 2005.

975 Zhao, R., Lee, A. K. Y., Huang, L., Li, X., Yang, F., and Abbatt, J. P. D.: Photochemical processing of  
976 aqueous atmospheric brown carbon, *Atmos. Chem. Phys.*, 15, 6087-6100, 10.5194/acp-15-6087-2015,  
977 2015.

978

979

980 **Table 1.** Initial gaseous and particle phase experimental conditions.

Exp. No. <sup>a</sup>	VOC	$c_{\text{VOC}}$ (ppbv)	$c_{\text{O}_3}$ (ppbv)	$c_{\text{OH}}$ (molecules $\text{cm}^{-3}$ )	$c_{\text{NH}_3}$ (ppbv)	$\text{H}_2\text{SO}_4/\text{Na}_2\text{SO}_4$ (mol/mol)	$c_{\text{P}}$ (particle $\text{cm}^{-3}$ )	$M_{\text{O}}^{\text{b}}$ ( $\mu\text{g m}^{-3}$ )
P1	$\alpha$ -pinene	11.7	30.7	$2.85 \times 10^6$	50.7	0.76	5863	11.2
P2	$\alpha$ -pinene	16.9	30.2	$1.77 \times 10^6$	66.6	1.19	5627	16.4
P3	$\alpha$ -pinene	22.1	30.0	$3.41 \times 10^6$	34.1	2.12	5377	23.5
P4	$\alpha$ -pinene	13.6	31.2	$2.81 \times 10^6$	40.6	1.71	4761	13.6
P5	$\alpha$ -pinene	13.3	33.4	$2.22 \times 10^6$	49.7	0	3836	5.8
P6	$\alpha$ -pinene	13.6	33.3	$1.57 \times 10^6$	40.8	1.68	5276	13.6
B7	–	0	31.8	–	44.0	1.68	4656	0.4
P8	$\alpha$ -pinene	11.9	33.1	$1.87 \times 10^6$	34.1	1.95	4632	12.8
P9	$\alpha$ -pinene	11.2	31.0	$2.18 \times 10^6$	42.6	1.95	5554	10.4
P10	$\alpha$ -pinene	11.3	31.0	$3.01 \times 10^6$	56.6	1.95	5437	15.4
P11	$\alpha$ -pinene	11.2	31.0	$2.41 \times 10^6$	63.9	1.95	5464	14.6
P12	$\alpha$ -pinene	12.8	30.9	$3.47 \times 10^6$	101.5	1.95	5495	20.6
P13	$\alpha$ -pinene	10.4	31.2	$3.41 \times 10^6$	75.1	1.95	5402	16.6
P14	$\alpha$ -pinene	10.9	29.2	$3.49 \times 10^6$	61.9	1.95	5809	15.6
M15	m-xylene	21.6	–	$1.74 \times 10^6$	49.4	1.95	4910	6.4
M16	m-xylene	25.0	–	$1.82 \times 10^6$	66.2	1.95	4966	6.8
M17	m-xylene	23.3	–	$1.78 \times 10^6$	86.2	1.95	4948	6.0
M18	m-xylene	21.1	–	$1.40 \times 10^6$	97.9	1.95	4612	5.4
M19	m-xylene	22.1	–	$1.93 \times 10^6$	104.4	1.95	4918	5.8
M20	m-xylene	19.7	–	$1.31 \times 10^6$	125.7	1.95	5248	5.6

981 <sup>a</sup> P, B and M represent  $\alpha$ -pinene, blank and m-xylene, respectively. Experiments performed at982 RH=50 $\pm$ 1 %; T=295 $\pm$ 2 K b. Organics after 6h of exposure

983

984

985

**Table 2.** Contribution of NOC to SOA and Total Nitrogen containing mass

Exp. No. <sup>a</sup>	VOC	SOA yield (%)	( $\gamma_{\text{limi}}$ ) <sup>b</sup>	N/C	C <sub>x</sub> H <sub>y</sub> N <sub>n</sub> /T <sub>NOC</sub> <sup>c</sup> (%)	C <sub>x</sub> H <sub>y</sub> ON <sub>n</sub> /T <sub>NOC</sub> <sup>c</sup> (%)	C <sub>x</sub> H <sub>y</sub> O <sub>2</sub> N <sub>n</sub> /T <sub>NOC</sub> <sup>c</sup> (%)	NO <sub>x</sub> /T <sub>NOC</sub> <sup>c</sup> (%)	NOC/TN (%) <sup>d</sup>	N <sub>NOC</sub> /N <sub>TN</sub> <sup>d</sup> (%) <sup>e</sup>	T <sub>NOC</sub> <sup>c</sup> /SOA (%) <sup>f</sup>
P1	$\alpha$ -pinene	22.1	$1.64 \pm 0.07 \times 10^{-3}$	$1.3 \times 10^{-2}$	15.1	11.8	11.1	62.0	18.5	8.7	11.0
P2	$\alpha$ -pinene	23.3	$2.00 \pm 0.58 \times 10^{-3}$	$1.3 \times 10^{-2}$	19.9	14.1	18.1	47.9	17.3	7.3	9.3
P3	$\alpha$ -pinene	26.0	$5.47 \pm 0.23 \times 10^{-3}$	$1.5 \times 10^{-2}$	30.0	19.8	15.5	34.6	18.5	7.7	8.2
P4	$\alpha$ -pinene	26.6	$5.21 \pm 0.16 \times 10^{-3}$	$2.3 \times 10^{-2}$	35.8	19.3	15.5	29.3	18.6	8.2	12.2
P5	$\alpha$ -pinene	11.6	$1.23 \pm 0.04 \times 10^{-3}$	$2.2 \times 10^{-2}$	40.8	24.6	16.9	17.7	40.1	19.2	9.0
P6	$\alpha$ -pinene	24.4	$3.05 \pm 0.11 \times 10^{-3}$	$1.8 \times 10^{-2}$	33.5	17.0	12.2	37.2	16.3	6.9	10.2
B7	-	-	-	-	-	-	-	-	-	-	-
P8	$\alpha$ -pinene	24.8	$4.02 \pm 0.18 \times 10^{-3}$	$2.1 \times 10^{-2}$	39.8	22.0	13.2	25.0	14.3	5.7	9.7
P9	$\alpha$ -pinene	20.8	$2.61 \pm 0.22 \times 10^{-3}$	$1.8 \times 10^{-2}$	32.3	19.3	20.8	27.7	12.2	4.7	9.2
P10	$\alpha$ -pinene	29.4	$1.78 \pm 0.07 \times 10^{-3}$	$1.5 \times 10^{-2}$	27.7	21.7	18.9	31.7	11.6	4.5	7.8
P11	$\alpha$ -pinene	28.0	$1.64 \pm 0.10 \times 10^{-3}$	$1.4 \times 10^{-2}$	29.4	21.8	15.4	33.4	10.1	3.9	7.1
P12	$\alpha$ -pinene	32.0	$1.62 \pm 0.09 \times 10^{-3}$	$1.5 \times 10^{-2}$	42.4	22.4	18.1	17.1	11.8	5.3	7.3
P13	$\alpha$ -pinene	31.8	$1.24 \pm 0.08 \times 10^{-3}$	$1.1 \times 10^{-2}$	29.5	17.3	19.1	34.1	11.5	4.5	6.2
P14	$\alpha$ -pinene	28.6	$1.53 \pm 0.06 \times 10^{-3}$	$1.4 \times 10^{-2}$	30.7	19.0	16.2	34.1	11.9	4.7	7.1
M15	m-xylene	12.6	$1.52 \pm 0.03 \times 10^{-2}$	$6.4 \times 10^{-2}$	34.3	15.7	4.5	45.6	23.1	10.0	28.9
M16	m-xylene	9.8	$8.21 \pm 0.30 \times 10^{-3}$	$5.6 \times 10^{-2}$	27.6	16.1	7.6	48.8	20.4	8.5	28.2
M17	m-xylene	9.8	$6.74 \pm 0.19 \times 10^{-3}$	$6.6 \times 10^{-2}$	32.7	17.6	3.6	46.1	20	8.6	30.1
M18	m-xylene	11.6	$4.00 \pm 0.11 \times 10^{-3}$	$7.6 \times 10^{-2}$	32.1	15.3	5.4	47.2	20.4	14	35.9
M19	m-xylene	9.4	$3.98 \pm 0.10 \times 10^{-3}$	$5.1 \times 10^{-2}$	24.4	14.8	6.2	54.6	16.3	11.8	27.5
M20	m-xylene	12.8	$4.10 \pm 0.13 \times 10^{-3}$	$7.9 \times 10^{-2}$	32.8	15.1	5.0	47.1	21.4	14.8	38.1
<b>Mean<math>\pm\sigma</math></b>			<b><math>4.0 \pm 3.3 \times 10^{-3}</math></b>		<b><math>31.1 \pm 6.7</math></b>	<b><math>18.1 \pm 3.4</math></b>	<b><math>12.8 \pm 5.7</math></b>	<b><math>38.0 \pm 12.1</math></b>	<b><math>17.6 \pm 6.7</math></b>	<b><math>8.4 \pm 4.1</math></b>	<b><math>16.0 \pm 11</math></b>

986



987 a. P, B and M represent  $\alpha$ -pinene, blank and m-xylene, respectively. b.  $\gamma$  leading to  $T_{\text{NOC}}$  derived  
988 excluding  $\text{NH}_x$  fragments. c. after 6 hours of exposure where  $T_{\text{NOC}} = \text{C}_x\text{H}_y\text{N}_n + \text{C}_x\text{H}_y\text{ON}_n +$   
989  $\text{C}_x\text{H}_y\text{O}_2\text{N}_n + \text{NO}_x$ . d. Where TN includes all nitrogen containing mass, including ammonium  
990 ( $\text{TN} = \text{C}_x\text{H}_y\text{N}_n + \text{C}_x\text{H}_y\text{ON}_n + \text{C}_x\text{H}_y\text{O}_2\text{N}_n + \text{NO}_x + \text{NH}_x$ ). e. Values given on a N atom/N atom  
991 mass basis. f. Ratio on a mass/mass basis

992 **Figure captions**

993 **Figure 1.** Typical HR-ToF-AMS spectra of (A) non-N-containing fragments and (B)

994 N-containing fragments in SOA formed by O<sub>3</sub> oxidation of α-pinene in the presence of

995 40.8 ppbv NH<sub>3</sub> (Exp. P5).

996 **Figure 2.** Infrared spectra for SOA from (A) ozonolysis of α-pinene (Exp. P11) and (B)

997 OH oxidation of m-xylene (Exp. M15) in the presence of NH<sub>3</sub>. *R* is the abbreviation for

998 reflectance in DRIFTS mode.

999 **Figure 3.** Concentration changes for N-containing fragments and SOA for (A)

1000 ozonolysis of α-pinene (Exp. P6) and (B) OH oxidation of m-xylene (Exp. M16),

1001 respectively; the relative fraction of each species to total NOC mass

1002 ( $T_{\text{NOC}} = C_xH_yN + C_xH_yON + C_xH_yO_2N + NO_x$ ) and T<sub>NOC</sub> to SOA fraction for (C) ozonolysis

1003 of α-pinene and (D) OH oxidation of m-xylene, respectively.

1004 **Figure 4.** Fitting of mass changes (Exp. P3 and P5) to derive uptake coefficients for

1005 NH<sub>3</sub> leading to T<sub>NOC</sub>. The red and blue lines represent the predicted values by the

1006 uptake model at the initial (from 0 to 150 min) and the final stages of the experiment

1007 (from 400 to 1250 min), respectively.

1008 **Figure 5.** Relationship between the  $\gamma_{t,\text{ini}}$  and particle-phase acidity when including

1009 (black) and excluding (red) NH<sub>x</sub> in the determination of  $\gamma$ . The error bars are derived

1010 from the uncertainties of the uptake model parameters

1011 **Figure 6.** Diffusion corrected uptake coefficient of NH<sub>3</sub> to form NOC species on SOA

1012 from O<sub>3</sub> oxidation of α-pinene (A) and OH oxidation of m-xylene (B), as a function of

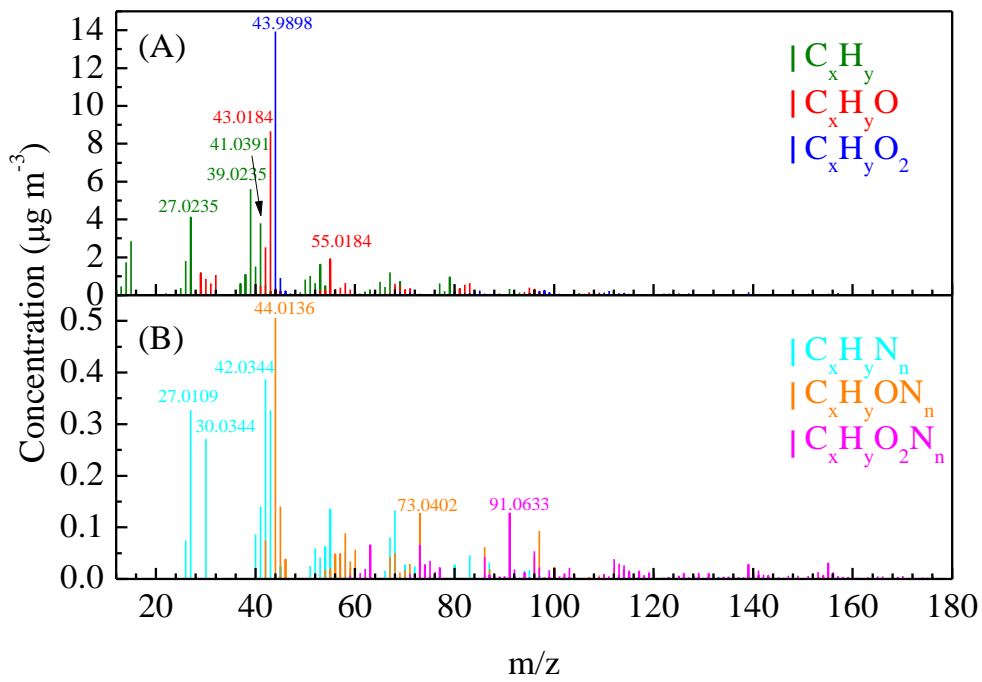
1013 NH<sub>3</sub> exposure (at fixed H<sub>2</sub>SO<sub>4</sub>/Na<sub>2</sub>SO<sub>4</sub> ratio; 1.95 mol/mol). This relationship is also

1014 shown for uptake coefficients derived including the NH<sub>x</sub> fragments (C) and (D). The

1015 error bars depict 1σ.

1016 **Figure 7.** Relative contribution of NOC to the total SOA (T<sub>NOC</sub>/SOA) as a function of

- 1017 organic mass loading for  $\alpha$ -pinene and m-xylene experiments at constant particle  
1018 acidity ( $\text{H}_2\text{SO}_4/\text{Na}_2\text{SO}_4$ : 1.95).

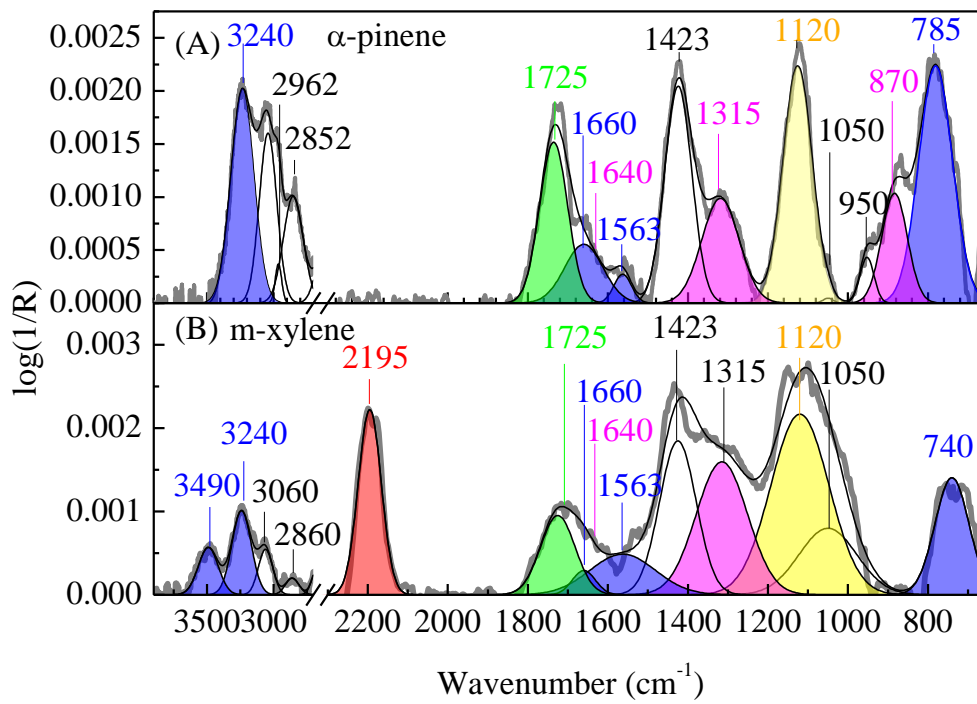


1020

1021

1022

**Figure 1.**



1024

1025

1026

1027

**Figure 2.**

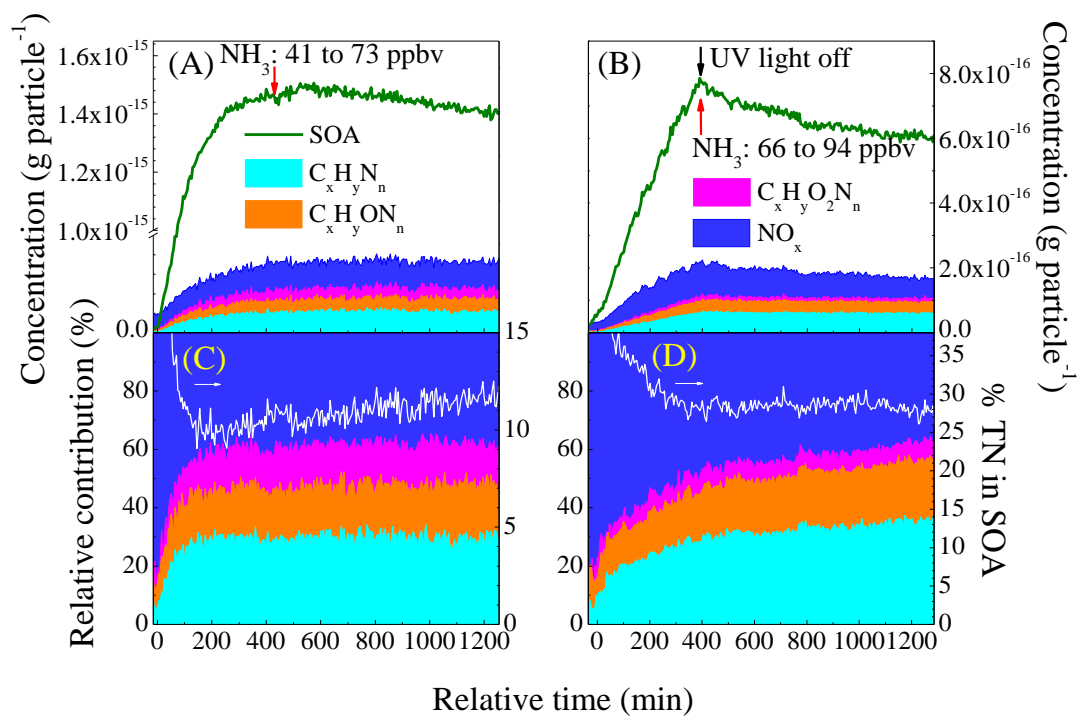


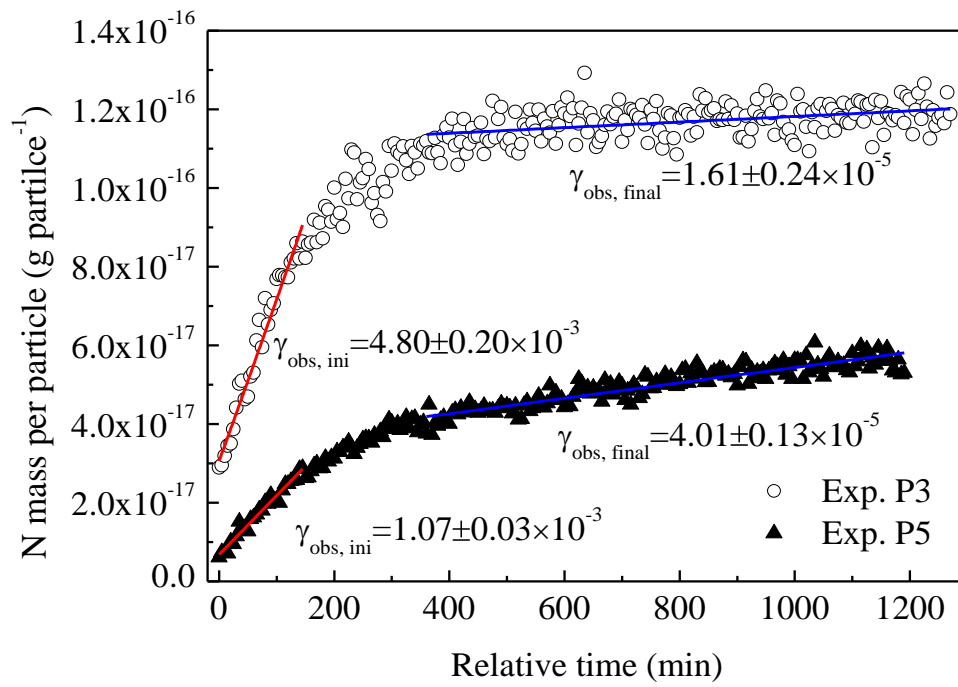
Figure 3.

1028

1029

1030

1031



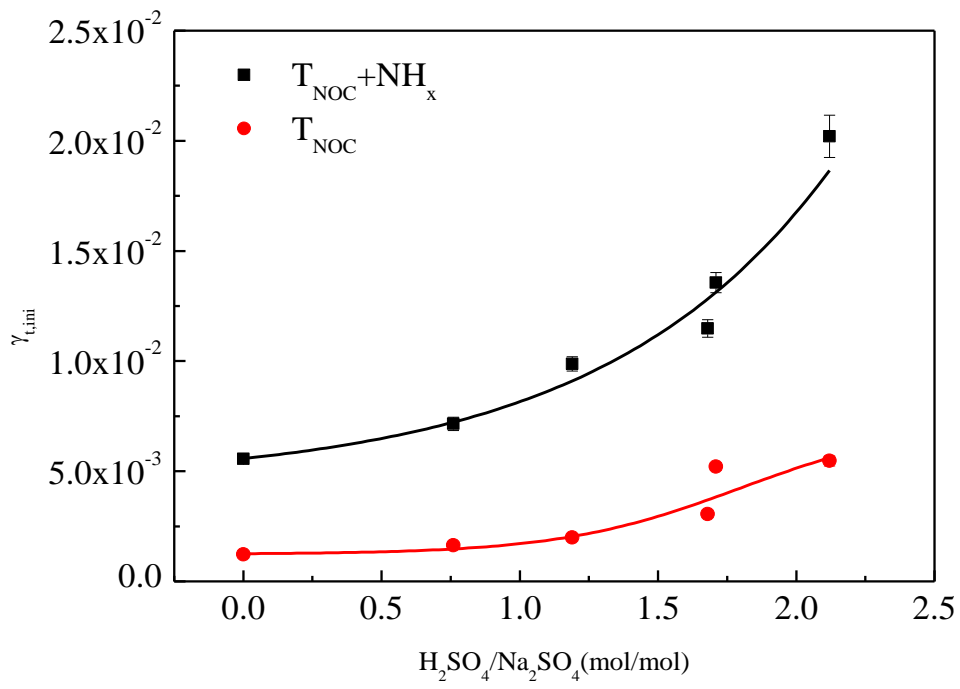
1032

1033

1034

**Figure 4.**

1035



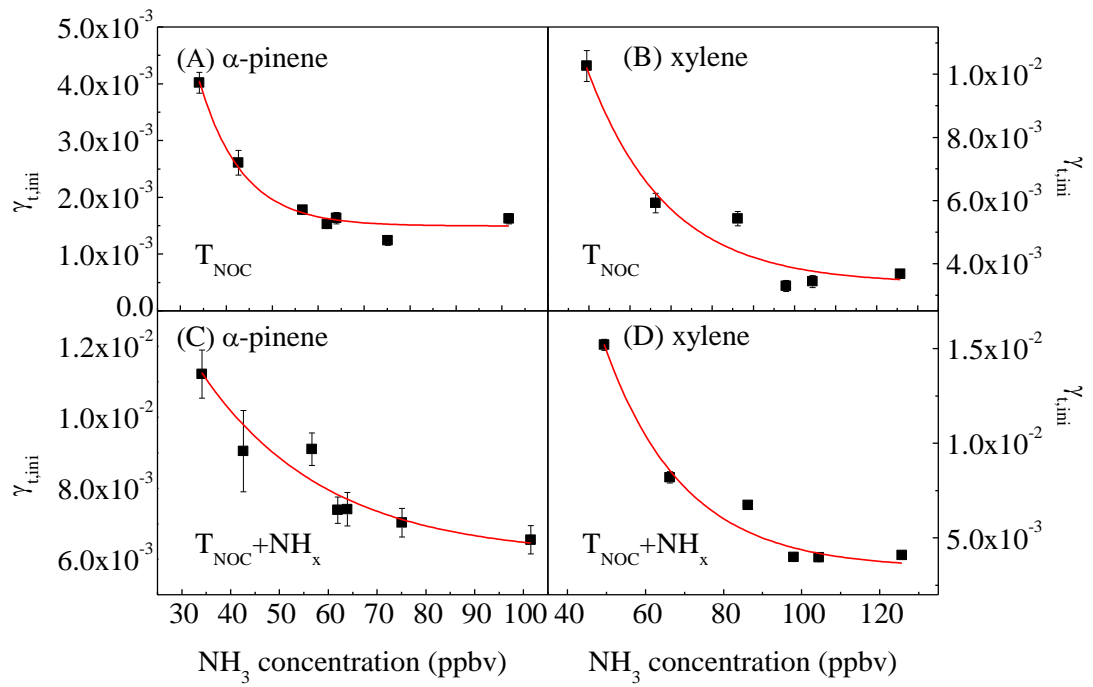
1036

1037

1038

**Figure 5.**



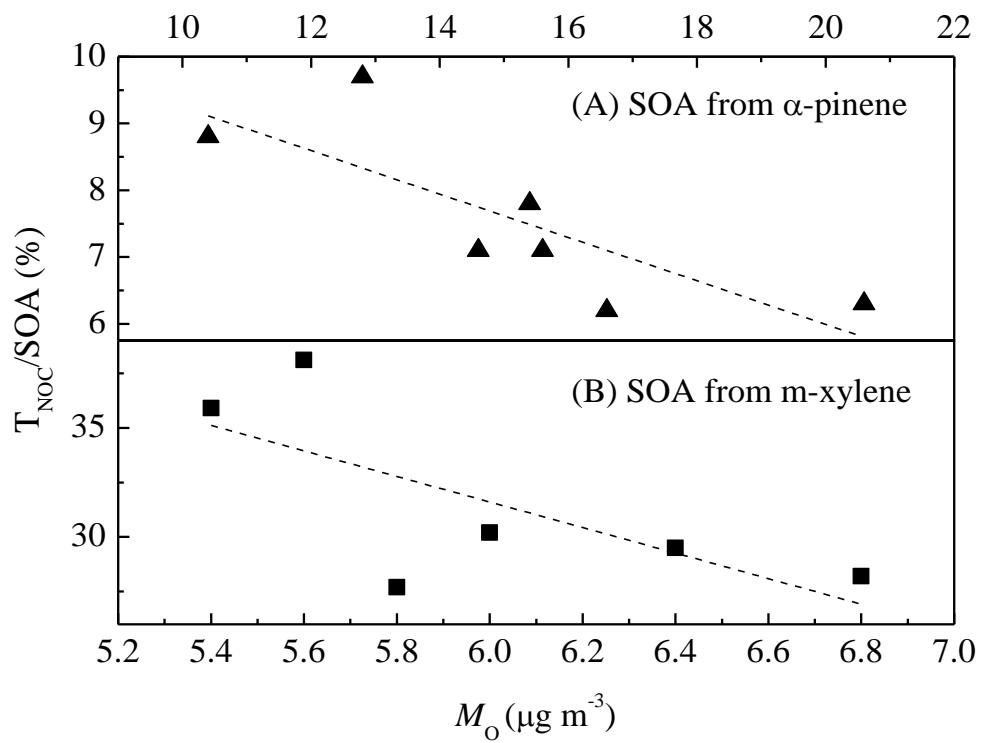


1040

1041

1042

**Figure 6.**



1043

1044

1045

1046

Figure 7